Characterization of CYP26B1-selective inhibitor, DX314, as a potential therapeutic for keratinization disorders

Veit, Joachim; DE GLAS, VALERIE; Balau, Benoit; Liu, Haoming; Bourlond, Florence; Paller, Amy; POUMAY, Yves; Diaz, Philippe

Published in:
The journal of investigative dermatology

DOI:
10.1016/j.jid.2020.05.090

Publication date:
2021

Document Version
Peer reviewed version

Characterization of CYP26B1-selective Inhibitor, DX314, as a Potential Therapeutic for Keratinization Disorders

Journal:	*Journal of Investigative Dermatology*
Manuscript ID	JID-2020-0105.R2
Article Type:	Original Article
Date Submitted by the Author:	29-Apr-2020
Complete List of Authors:	Veit, Joachim; University of Montana Missoula, Biomedical and Pharmaceutical Sciences De Glas, Valerie; University of Namur, URPHYM-NARLIS Balau, Benoît; University of Namur, URPHYM-NARLIS Liu, Haoming; Northwestern University Feinberg School of Medicine, Departments of Dermatology and Pediatrics Bourlond, Florence; Hôpital Erasme, Université Libre de Bruxelles, Service de Dermatologie Paller, Amy; Northwestern University Feinberg School of Medicine, Departments of Dermatology and Pediatrics Poumay, Yves; University of Namur, URPHYM-NARLIS Diaz, Philippe; University of Montana Missoula, Biomedical and Pharmaceutical Sciences; DermaXon LLC, R&D
Keywords:	Drug Development, Keratinization Disorders, Barrier Function, Pharmacology, Ichthyosis

Editor comments:

Section/Deputy Editor: 1

Comments to the Author:

Revision is responsive to reviewer comments and improved by revision.

- We would like to thank the editors for their time and feedback regarding our submission.

- The only change we are submitting in this revision is to a minor figure reference issue we found in the Figure 4 legend. The reference to parts "(a,c,d)" in the last sentence was changed to correctly read "(a,b,d)". This correction was highlighted and underlined in yellow in the manuscript text.

Reviewer comments:

Reviewer: 1

Comments to the Author

This is a very careful Revision of an excellent paper. My concern on the experimental design used, namely a simultaneous co-tratment with all trans retinoic acid in the keratinocyte cultures is well and fully adressed and authors Point out that in the rhino mice model no cotratment was used, but similar effects were achieved. Moreover, they clarify that in their in vitro conditions no RA precursors and no appreciable levels of all trans retinoic acid will be present which justifies their Approach and they provide several prominent references like that of Giltaire et al 2009 on this culture model. All specific points have been fully and carefully adressed. No further comment.

Reviewer: 2

Comments to the Author

I believe that the authors have responded adequately to my questions.

- We would like to sincerely thank reviewer #1 and reviewer #2 for their time, effort and comments regarding our submission.

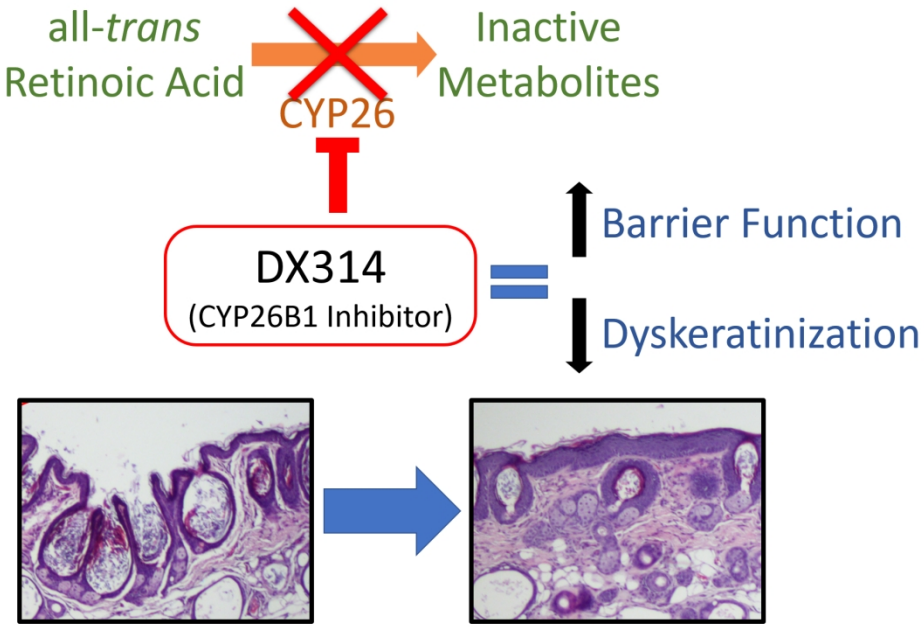

527x355mm (96 x 96 DPI)

Informative Title:

Characterization of CYP26B1-selective Inhibitor, DX314, as a Potential Therapeutic for Keratinization Disorders

Short Title:

DX314: Keratinization Disorder Therapeutic

Joachim G.S. Veit[1], Valérie De Glas[2], Benoît Balau[2], Haoming Liu[4], Florence Bourlond[5], Amy S. Paller[4], Yves Poumay[2], Philippe Diaz[1,3]

[1]Department of Biomedical and Pharmaceutical Sciences, University of Montana, Missoula, MT
[2]URPHYM-NARLIS, University of Namur, Namur, Belgium
[3]DermaXon LLC, Missoula, MT
[4]Departments of Dermatology and Pediatrics, Northwestern University Feinberg School of Medicine, Chicago, IL
[5]Service de Dermatologie, Hôpital Erasme, Université Libre de Bruxelles, Belgique

Correspondence: Philippe Diaz, Department of Biomedical and Pharmaceutical Sciences, University of Montana, 32 Campus Dr., Missoula, MT, 59812. Email: philippe.diaz@umontana.edu

ORCIDs:
Joachim G.S. Veit: https://orcid.org/0000-0001-5908-0648
Valérie De Glas: https://orcid.org/0000-0001-7366-2601
Benoît Balau: https://orcid.org/0000-0002-7314-860X
Haoming Liu: https://orcid.org/0000-0002-3190-5422
Florence Bourlond: https://orcid.org/0000-0003-1071-3306
Amy S. Paller: https://orcid.org/0000-0001-6187-6549
Yves Poumay: http://orcid.org/0000-0001-5200-3367
Philippe Diaz: https://orcid.org/0000-0002-2339-8803

Abbreviations: RAMBA, retinoic acid metabolism blocking agents; a*t*RA, all-*trans*-retinoic acid; RHE, reconstructed human epidermis; TEER, transepithelial electrical resistance; TEWL, transepidermal water loss; CYP26, cytochrome p450 family 26; DD, Darier disease; LI, lamellar ichthyosis; RXLI, Recessive x-linked ichthyosis. See supplementary materials for additional abbreviations (**Table S4**)

Funding: This work was supported by the by the National Institute of Arthritis and Musculoskeletal and Skin Disease of the National Institutes of Health: R44AR069416 (PD), P20GM103546 (PD, JV). The content of this paper is solely the responsibility of the authors and does not necessarily reflect the official views of the National Institutes of Health.

ABSTRACT

Inhibition of cytochrome P450 (CYP)-mediated retinoic acid (RA) metabolism by RA metabolism blocking agents (RAMBAs) increases endogenous retinoids and is an alternative to retinoid therapy. Currently available RAMBAs (i.e. liarozole and talarozole) tend to have fewer adverse effects than traditional retinoids but lack target specificity. Substrate-based inhibitor DX314 has enhanced selectivity for RA-metabolizing enzyme CYP26B1 and may offer an improved treatment option for keratinization disorders such as congenital ichthyosis and Darier disease. In this study we use RT-qPCR, RNA sequencing, pathway, upstream regulator, and histological analyses to demonstrate that DX314 can potentiate the effects of all-*trans*-RA (a*t*RA) in healthy and diseased reconstructed human epidermis (RHE). We unexpectedly discovered that DX314, but not a*t*RA or previous RAMBAs, appears to protect epidermal barrier integrity. Additionally, DX314-induced keratinization and epidermal proliferation effects are observed in a rhino mice model. Altogether, results indicate that DX314 inhibits a*t*RA metabolism with minimal off-target activity and shows therapeutic similarity to topical retinoids *in vitro* and *in vivo*. Findings of a unique barrier-protecting effect require further mechanistic study but may lead to a novel strategy in barrier-reinforcing therapies. DX314 is a unique and promising candidate compound for further study and development in the context of keratinization disorders.

INTRODUCTION

Therapeutics targeting retinoid biopathways have been implemented in the clinical treatment of keratinization disorders such as the congenital ichthyoses (Vahlquist et al. 2008), Darier disease (DD) (Casals et al. 2009; Cooper and Burge 2003; Dicken et al. 1982; Steijlen et al. 1993), and other skin disorders (e.g. acne, psoriasis) (Dawson and Dellavalle 2013; Fisher and Voorhees 1996) to alleviate patient symptoms. Such therapies leverage the role of endogenous retinoids in regulating keratinocyte proliferation and differentiation. Retinoid bioactivity is primarily, although not solely, mediated by transcription factors such as retinoic acid receptors (RAR) and retinoid X receptors (RXR) (Fisher et al. 1994).

However, retinoid treatments also result in adverse effects including dry skin, irritation, redness, photosensitivity, teratogenicity and barrier impairment (Orfanos et al. 1997). Endogenously-occurring retinoids (e.g. tretinoin) autoinduce their own metabolism (Van Der Leede et al. 1997; Marikar et al. 1998), which in turn demands higher exogenous doses for effective treatment, resulting in increased systemic exposure. Synthetic retinoids, particularly tazarotenic acid, will both activate RARs and inhibit RA-metabolism (Foti et al. 2016), which may overstimulate retinoid biopathways and increase associated adverse effects. For these reasons, RA metabolism blocking agents (RAMBAs) (Verfaille et al. 2008), including liarozole and talarozole, were developed to target the primary RA-specific metabolizing enzymes of the cytochrome p450 family 26 (CYP26) (Ray et al. 1997).

RAMBAs, particularly when used topically, achieve therapeutic effects without high exposure to systemic levels of RA by utilizing endogenously available RA rather than high doses of exogenous retinoids, which theoretically reduces overexposure and adverse effects. Topical RAMBAs could be implemented either as standalone treatments or as adjunct therapies to reduce

oral retinoid dosing without loss of therapeutic efficacy. Reports illustrate successful inhibition of RA metabolism using liarozole (Van Wauwe et al. 1992) and proven efficacy in treating several skin disorders (Berth-Jones et al. 2000; Bhushan et al. 2001; Kang et al. 1996; Kuijpers et al. 1998; Lucker et al. 2005; Lucker et al. 1997; Vahlquist et al. 2014), including in a comparative trial vs acitretin (an oral retinoid) for congenital ichthyosis, which showed a trend towards a better safety profile (Verfaille et al. 2007b). Problematically, liarozole also inhibits off-target CYPs such as aromatase (CYP19), an important enzyme in estradiol biosynthesis (Nelson et al. 2013). Previous RAMBAs have not progressed past clinical trials, suggesting the need for improved RAMBA candidates.

The promising results of early-generation RAMBAs led Diaz et al. to develop a series of compounds targeting RA metabolism *via* specific inhibition of two CYP26 isoforms (A1 and B1) (Diaz et al. 2016). Removal of the heme-interacting azole moiety, thought to contribute to the non-specific effects of previous azole-containing RAMBAs, may preserve the desired effects while minimizing off-target activity. One of these compounds, a CYP26B1-specific inhibitor, DX314 (IC_{50}: CYP26A1=1752nM; CYP26B1=108nM), was described in US patent US009963439B2 as example 39 (Diaz et al. 2018).

Endogenous all-*trans*-RA (a*t*RA) is a well-known regulator of epidermal proliferation and differentiation (Fisher and Voorhees 1996), in part by inducing heparin-binding EGF-like growth factor (HBEGF), which stimulates keratinocyte proliferation (Rittié et al. 2006; Stoll and Elder 1998; Xiao et al. 1999; Yoshimura et al. 2003), and involucrin (IVL), a late marker of epidermal differentiation (Eckert et al. 2004; Monzon et al. 1996; Poumay et al. 1999). Expression of both CYP26A1 and CYP26B1 is induced by a*t*RA, but only the CYP26A1

promotor contains a RA response element (RARE) which directly binds RARs (Pavez Loriè et al. 2009a).

In this study, we investigate RAMBAs *in vitro* under tightly-controlled growth conditions that specifically do not contain RA or RA precursors (Giltaire et al. 2009; Minner et al. 2010; Pavez Loriè et al. 2009a; Poumay et al. 1999). In these conditions, a highly specific RAMBA will have a negligible effect in the absence of a*t*RA, however when co-treated with a nanomolar dose of a*t*RA, facilitate a relative increase in a*t*RA concentration by inhibiting its metabolism, and therefore potentiate the expression of RA-responsive genes. Since *in vivo* concentrations of a*t*RA in healthy human skin are typically 2-4nM (Mihály et al. 2011), we co-treated RAMBAs *in vitro* with 1nM a*t*RA to provide a near-physiological basal level, without saturating nanomolar-sensitive a*t*RA effects, which allowed us to observe if RAMBAs can potentiate those effects.

Skin acts as an effective barrier to the environment. Changes in epidermal barrier integrity can be investigated using transepithelial electrical resistance (TEER) and transepidermal water loss (TEWL). TEER is an *in vitro* assay assessing electrical properties to evaluate possible changes in trans- and paracellular (regulated by tight junctions) ion permeability across the epidermis. TEWL measures passive diffusion of water across the epidermis and can be performed *in vivo* or *in vitro*. Decreased TEER or increased TEWL typically indicates barrier integrity disruption.

Our data show that DX314 potentiates the effects of a*t*RA on gene expression in healthy and diseased epidermis by inhibiting CYP26B1-mediated RA metabolism. Unexpectedly, DX314 mitigated the epidermal barrier dysregulation and irregular morphology displayed by other RAMBAs and high dose a*t*RA. In addition, topical DX314 induced comedolytic/anti-

keratinizing effects in the rhino mouse model, reflecting those observed in previous retinoid studies (Ashton et al. 1984; Fort-Lacoste et al. 1999; Kligman and Kligman 1979).

Together, this study suggests that DX314 exhibits potential as a new keratinization disorder therapeutic that may address some shortcomings of previous retinoid-based treatments.

RESULTS

DX314 potentiates the effects of a*t*RA in healthy and keratinization disorder keratinocytes

Based on RT-qPCR assays, a 4-day a*t*RA treatment of RHE caused a dose-dependent increase in HBEGF, CYP26A1 and IVL gene expression (**Figure 1a**). DX314, together with near-physiological dosing of a*t*RA (1nM; to provide basal RA without saturating sensitive RA pathways) mimics the consequences of high dose a*t*RA on the expression of every gene analyzed, indicating potentiation of a*t*RA. Liarozole with a*t*RA significantly increases HBEGF and CYP26A1 expression relative to control, but only CYP26A1 expression is potentiated compared to 1nM a*t*RA alone.

Immunostaining shows IVL (**Figure 1b**) primarily localized in the upper epidermis of control and DX314-alone RHE. Induction of early IVL expression is observed in basal and suprabasal layers of the epidermis with a*t*RA-alone, and even more so, DX314 with 1nM a*t*RA.

RNAseq confirmed that DX314 alone (a*t*RA-free conditions) had no effect on HBEGF, IVL, CYP26A1 or CYP26B1 mRNA expression (**Figure 1c**), and that DX314 potentiated the effects of 1nM a*t*RA, not only on these genes, but on numerous other known retinoid-responsive genes, among them several keratins (KRT) (Radoja et al. 1997), lecithin:retinol acyl-transferase (LRAT) (Kurlandsky et al. 1996), retinol binding protein 1 (RBP1) (Kang et al. 1995), and cellular retinoic acid binding protein 2 (CRABP2) (Aström et al. 1994). Changes in expression of

other genes that involve both direct (RARE-containing promotor, indicated by adjacent green box) (Aström et al. 1992; Fisher et al. 1995; Lalevée et al. 2011; Laursen et al. 2015; Loudig et al. 2000; Radoja et al. 1997; de Thé et al. 1990; Tomic-Canic et al. 1992; Vasios et al. 1989) and indirect or unknown RA pathways supported the potentiation effect.

RNAseq data was further analyzed with Ingenuity Pathway Analysis (IPA) (Krämer et al. 2014) software for canonical pathway and upstream regulator prediction. The applied significance cutoffs (see **Methods**) resulted in 1360, 5480, 169, and 3015 differentially expressed genes in RHE treated with 1nM a*t*RA, 100nM a*t*RA, 1000nM DX314, and 1000nM DX314 with 1nM a*t*RA, respectively. Analysis results were sorted by overall |z-score|, indicating the strength and direction of each prediction (positive score = activation, negative score = inhibition). As expected, the upstream regulator with largest activation score was a*t*RA (tretinoin), which displayed an activation pattern consistent with a*t*RA potentiation (**Figure 1d**). Of the top 20 scoring regulators, only three weakly displayed any predicted activity by DX314 alone. Canonical pathway analysis (**Figure 1e**) found the overall most activated ("Integrin Signaling") and inhibited ("RhoGDI Signaling") pathways both display activation patterns suggesting a potentiation of a*t*RA by DX314.

To test the potential of DX314 in certain keratinization disorders, we investigated CYP26A1 gene expression in keratinocytes from patients with Darier disease (DD), recessive x-linked ichthyosis (RXLI), and lamellar ichthyosis (LI). DX314 potentiates the effects of a*t*RA in DD RHE (**Figure 2a**), RXLI full-thickness RHE (**Figure 2b**), LI RHE (**Figure 2c**), and RXLI monolayer cultures (**Figure 2d**). Talarozole potentiated a*t*RA in DD RHE and liarozole potentiated a*t*RA in RXLI full-thickness RHE.

Histological analysis shows that a*t*RA induces robust morphological changes in DD RHE (**Figure 3a**) including a dramatic loss of SG (and their filaggrin-containing keratohyalin granules (KG)), denucleation and flattening of stratum spinosum (SS) keratinocytes, and an overall unhealthy appearance. When treated alone, DX314 and talarozole caused no major morphological changes. Co-treatment with talarozole and 1nM a*t*RA shifted the cell morphology, most notably with loss of SG and flattening of epidermal keratinocytes, to more closely resemble the appearance of high dose a*t*RA. DX314 with a*t*RA also affected morphology relative to DX314 alone, but to a lesser extent, with the appearance not significantly different than control or only 1nM a*t*RA-treated RHE.

KRT10, a commonly used marker of epidermal differentiation that localizes to the suprabasal epidermis, showed reduced expression in a*t*RA-treated RHE (**Figure 3b**). Treatment with DX314 or talarozole alone led to no change in KRT10 localization, but co-treatment with near-physiological levels of a*t*RA reduced staining in the lower SS. KRT10 gene expression in DD RHE (**Figure 3c**) was decreased by a*t*RA in a dose-dependent manner and was potentiated by DX314 and talarozole. This effect on KRT10 was also observed in healthy RHE (**Figure 1c** and **S1**).

DX314 induces barrier effects in healthy and diseased RHE

As a measure of barrier integrity, TEER of healthy RHE was assessed. Independent runs with RHE from several donors were pooled and normalized to their respective controls (**Figure 4a**). High dose a*t*RA significantly decreased TEER. Liarozole and talarozole alone showed no effect on TEER, but co-treatment with a*t*RA resulted in significant TEER decrease. Surprisingly, in both healthy and LI (**Figure 4b**) RHE, DX314 alone increased TEER and caused no decrease

relative to control with a*t*RA co-treatment. TEWL was similarly affected by a*t*RA, but no significant change was seen with DX314 alone.

Morphologically, a*t*RA disrupted LI (**Figure 4c**) and healthy RHE (**Figure S2** and **S3**) structure as described above. DX314 led to no major changes in morphology when dosed alone. However, unlike other RAMBAs (**Figure S2**), DX314 with a*t*RA co-treatment reduced disruption in normal morphology (improved SG/KG, more columnar basal keratinocytes, and less disorganized upper epidermis). Semi-quantitative analysis of SG surface area (**Figure 4d**), measured in healthy RHE (**Figure S3**), confirmed a dramatic reduction of the SG by a*t*RA, but no significant loss in DX314 treated groups.

The epidermal differentiation complex (EDC) is a cluster of genes on human locus 1q21 that are essential for epidermal differentiation (Kypriotou et al. 2012). As noted using RNAseq, expression of these genes (**Figure 4e**) is generally consistent with other retinoid-responsive genes. However, many cornified envelope (CE) precursor family genes, such as late cornified envelope (LCE) and small proline rich (SPRR) proteins, were dramatically downregulated by high dose a*t*RA, but not affected by DX314 with a*t*RA, which may play a role in the observed barrier effects. In addition, FLG expression was increased 2-fold with the DX314-a*t*RA combination, but not with high dose a*t*RA.

Nuclear receptor profiling revealed that DX314 acts as an inverse agonist for RAR-related orphan receptors (ROR) α and γ (**Figure S4**), while showing no activity on any other nuclear receptors studied.

DX314 reduces epidermal abnormalities in rhino mice

Rhino mice are commonly used as an *in vivo* model for screening comedolytic and anti-keratinizing compounds such as retinoids (Ashton et al. 1984; Fort-Lacoste et al. 1999; Griffiths

et al. 1993; Seiberg et al. 1997). Overall, DX314 treatment improved skin morphology (**Figure 5**). DX314 decreased comedo density (**Figure 6a** and **6b**), increased the mean comedo profile (ratio of comedo opening size to internal diameter) (**Figure 6c**), suggesting comedolysis, and induced epidermal thickening (**Figure 6d**), consistent with previous studies of topical retinoids. Again, DX314 treatment did not change TEWL relative to vehicle (**Figure 6e**). No abnormal behavior, adverse skin changes, changes in body weight or DRAIZE scoring (**Table S5** and **S6**) were observed throughout the study.

DISCUSSION

Retinoid-based drugs are well-accepted therapeutics for the treatment of many skin diseases (Dawson and Dellavalle 2013; Fisher and Voorhees 1996; Vahlquist et al. 2008). Despite their efficacy, use often leads to adverse reactions from their wide spectrum of non-therapeutically relevant endogenous roles, which are exacerbated by metabolic autoinduction and tolerance (Digiovanna et al. 2013; Orfanos et al. 1997). A strategy involving RAMBAs showed potential in preclinical and clinical studies (Berth-Jones et al. 2000; Bhushan et al. 2001; Bovenschen et al. 2007; Giltaire et al. 2009; Kang et al. 1996; Kuijpers et al. 1998; Lucker et al. 2005; Lucker et al. 1997; Pavez Lorié et al. 2009b; Stoppie et al. 2000; Vahlquist et al. 2014; Verfaille et al. 2007a; Van Wauwe et al. 1992), however, first-generation RAMBAs have not progressed to approved for clinical use. A highly selective RAMBA, with low risk of adverse events, could address the downsides of current treatment options. This study investigates the CYP26B1-selective compound, DX314, as a potential next-generation RAMBA.

Potentiation of the effects of a low, physiologically relevant dose of a*t*RA by DX314 in healthy and keratinization disorder keratinocytes, but not DX314 in an a*t*RA-free environment,

confirms that DX314 acts by inhibiting a*t*RA metabolism. These gene expression patterns were reproduced in keratinocyte cultures from individuals with DD and congenital ichthyosis, in addition to healthy skin, suggesting that the bioactivity of DX314 can be therapeutically relevant in skin disorders.

A broader investigation of gene expression changes using RNAseq also showed a strong pattern indicating potentiation of a*t*RA by DX314 on both RARE-promoted, and indirectly regulated genes. Pathway analysis found compelling supporting evidence in predicted upstream regulator and canonical pathway activation patterns.

Immunostaining confirmed the a*t*RA potentiating effects of DX314 on IVL localization in healthy RHE and KRT10 localization in DD RHE.

These experiments showed that DX314 alone had minimal effect on gene expression and therefor, minimal potential for off-target adverse effects, despite therapeutically relevant effects when paired with endogenous levels of a*t*RA.

Keratinization disorders are associated with intrinsic epidermal barrier disruption and a therapy that improves barrier function would be highly desirable. Surprisingly, this study found a significant increase in TEER compared to controls in RHE treated with DX314 alone, and unlike with liarozole and talarozole, no decrease from control when co-treated with a*t*RA. Although higher doses of a*t*RA significantly decreased TEER and DX314 otherwise appeared to potentiate the effects of a*t*RA, DX314 with a*t*RA did not impair barrier function below that of the control. TEWL in LI RHE, which is expected to increase with retinoid treatment or ablation of CYP26B1 (Okano et al. 2012), was not increased by DX314 alone or beyond that of 1nM a*t*RA when added as co-treatment. DX314 did not decrease TEWL in RHE, however, a lack of correlation between *in vitro* TEWL and barrier function has been previously documented (Chilcott et al. 2002).

Despite previous studies in rhino mice showing retinoids inducing substantial increases in TEWL (Elias et al. 1981; Gendimenico et al. 1994), our study found a slight, albeit a non-significant, decrease in TEWL, which additionally suggests an *in vivo* barrier-protecting effect.

Morphologically, DX314-treated RHE show dramatically less disruption of the SG and KG, and display an overall healthy appearance compared to a*t*RA, liarozole or talarozole-treated healthy, DD, and LI RHE. Semi-quantitative analysis of SG surface area also showed a significant decrease in a*t*RA-treated RHE, but no significant change in RHE treated with DX314, with or without a*t*RA. Nevertheless, DX314-treated RHE tissue sections had a more continuous SG/KG layer relative to controls, which may translate to an increase in TEER.

We observed minimal changes in the expression of many cornified envelope precursor proteins within the EDC, despite a large decrease in expression by high dose a*t*RA and DX314 potentiating of the effects of a*t*RA on other retinoid-responsive genes. We speculate that this preservation of CE protein expression may contribute to the ameliorative effect of DX314 on barrier integrity. In addition, DX314 displays unique inverse agonist activity on RORα and γ. Affinity for RORγ may be explained by DX314's structural similarity to a*t*RA, which has been previously shown to bind to, and inhibit, RORγ (Stehlin-Gaon et al. 2003). Conversely, a*t*RA was not found to act on ROR*a*, so the DX314 inverse agonism represents another unique property. Furthermore, a previously studied topical ROR*a/*γ inverse agonist was found to inhibit inflammation in mouse models of atopic dermatitis (Dai et al. 2017), a skin disorder displaying pathological barrier disruption. Future investigations should explore the potential link between DX314's ROR*a/*γ activity and its barrier effects, as well as potential contribution to therapeutic effects of skin barrier protection.

Use of rhino mice to study the *in vivo* effects of dermatologically active compounds such as retinoids is well-established, and unlike *in vitro,* does not require co-treatment with a*t*RA since adequate RA is generated *in vivo* through dietary sources. Reduction of the acne-like cysts (comedones), as well as the associated epidermal thickening (hyperplasia), are sensitive to retinoid treatment. In this preliminary study, DX314 led to significant improvement overall in comedo number (comedones per cm of skin), profile, and induced epidermal thickening. Optimization of the DX314 formulation (to eliminate the harsh acetone vehicle), dosing to improve bioavailability, and extending the treatment duration are likely to amplify DX314 efficacy in this model.

We conclude that our results provide strong evidence that DX314, which is known to specifically inhibit the RA-metabolizing enzyme CYP26B1, potentiates the effects of physiological levels of a*t*RA in keratinocytes from healthy skin and keratinization disorders *in vitro*; may protect from epidermal skin barrier disruption by retinoids; and has a restorative effect on changes *in vivo* rhino mouse skin consistent with previous retinoid treatments. These observations merit further investigation as a unique keratinization disorder treatment with the ability to simultaneously correct abnormal keratinization while protecting critical skin barrier function. Together these findings present an exciting new therapeutic candidate aimed at providing improved patient outcomes with minimal adverse effects, in contrast to currently available treatments.

MATERIALS AND METHODS

Primary keratinocytes

Healthy and DD primary keratinocytes, provided by Dr. Poumay's lab (Namur, Belgium), were isolated as previously described (Poumay et al. 2004) from skin samples provided by Drs. B. Bienfait and J.S. Blairvacq (Clinique St Luc, Namur-Bouge, Belgium). Additional healthy keratinocytes were purchased from ThermoFisher (Cascade Biologics, Portland, OR). RXLI and LI keratinocytes were provided by Dr. Paller (Northwestern University, IL). Details in **Table S1**.

Monolayer culture and RHE

Monolayer cultures were prepared as previously described (Minner et al. 2010). Upon reaching confluence, keratinocytes were treated for 20hr to compounds solubilized in media (0.1% DMSO vehicle for all *in vitro* studies).

RHE were produced as previously described (Poumay et al. 2004; De Vuyst et al. 2014) in Epilife media with 1.5mM Ca^{2+} (Cascade Biologics, Portland, OR), 10ng/mL keratinocyte growth factor (Sigma, Saint Louis, MO) and 50µg/mL vitamin C (Sigma, Saint Louis, MO). Treatments were started day 7 of growth, refreshed day 9, and halted day 11.

Full-thickness RHE were prepared as previously described (Zheng et al. 2012). Briefly, keratinocytes were seeded atop a simulated dermis (collagen matrix containing J2-3T3 fibroblasts) and allowed to develop into stratified epidermis before receiving a 4-day treatment (refreshed day 2).

RHE histological analysis and immunostaining

RHE were processed as previously described (Frankart et al. 2012; De Vuyst et al. 2014) and stained with hematoxylin-eosin (HE) or prepared for immunostaining. Further described in **Supplementary Methods**.

Measures of epidermal barrier function

TEER was measured by a previously described method (Frankart et al. 2012) with a ERS-2 voltohmmeter (Millipore, Burlington, MA). TEWL measurement used an AquaFlux AF200 evaporimeter (Biox Systems, London, England). For RHE, a sterilized gasket was placed between the cell culture insert and TEWL probe to form airtight seal. TEWL was measured over 60-90s until reaching a steady state. Analysis of SG surface area was performed using Fiji/ImageJ (Schindelin et al. 2012). SG surface area, defined by the presence of KG, was manually outlined and the area divided by each tissue's total area.

RNA isolation, RT-qPCR, RNAseq, and bioinformatics

Details on RT-qPCR, RNA-seq, and bioinformatics (Andrews 2010; Bolger et al. 2014; Durinck et al. 2009; Kim et al. 2017; Kim et al. 2016; Kim et al. 2015; Li et al. 2009; Love et al. 2013; Pertea et al. 2015; RCoreTeam 2018; Zhu et al. 2018) are provided in **Supplementary Methods**. Primer sequences (Giltaire et al. 2009) provided in **Table S2**.

When applicable, a method described by (Willems et al. 2008) was used to standardize the qPCR data to correct for interindividual variability before analysis.

Nuclear receptor profiling

Refer to **Supplementary Methods.**

Rhino mice

Eleven RHJ/LeJ rhino mice (2-3 males, 3 females per group) received daily topical application of 50μL vehicle (acetone), or 1% DX314, on a 2x2cm area of back skin for 11 days. All animal studies were approved by IACUC under NIH guidelines. Details in **Supplementary Methods**.

Statistical analysis

Statistics, apart from separately described RNAseq portion, were performed as described in respective figure legends using Prism 6 (Graphpad Software, La Jolla, CA).

Data availability statement

Data available upon request.

CONFLICTS OF INTEREST

PD is cofounder of DermaXon™ and inventor of the technology, he and The University of Montana are entitled to future royalty payments. JV was employed at DermaXon™ during a portion of this study.

ACKNOWLEDGMENTS

We would like to thank Drs. B. Bienfait and JS. Blairvacq (Clinique St. Luc, Namur-Bouge, Belgium) for providing skin samples used in this study. We would also like to thank Joanna Kreitinger and Larissa Walker of DermaXon™ and the Northwestern University Skin Biology and Diseases Resource-based Center (P30AR075049) for their assistance with various lab tasks.

AUTHOR CONTRIBUTIONS

Conceptualization: *lead*- PD; *equal*- JV, YP, AP
Data Curation: *lead*- JV
Formal Analysis: *lead*- JV
Funding Acquisition: *lead*- PD; *equal*- AP; *supportive*- JV
Investigation: *lead*- JV; *supportive*- VDG, BB, HL
Methodology: *equal*- JV, YP, PD; *supportive*- AP
Project Administration: *lead*- PD; *supportive*- JV, AP, YP
Resources: *equal*- JV, YP, PD; *supportive*- AP, VDG, BB, HL
Software: *lead*- JV
Supervision: *lead*- PD; *supportive*- AP, YP
Validation: *equal*- JV, YP, PD; *supportive*- FB
Visualization: *lead*- JV
Writing – Original Draft Preparation: *lead*- JV
Writing – Review and Editing: *equal*- JV, AP, YP, PD

REFERENCES

Andrews S. FastQC: A quality control tool for high throughput sequence data. [Internet]. 2010. Available from: https://www.bioinformatics.babraham.ac.uk/projects/fastqc/

Ashton RE, Connor MJ, Lowe NJ. Histologic changes in the skin of the rhino mouse (hrrhhrrh) induced by retinoids. J. Invest. Dermatol. Elsevier Masson SAS; 1984;82(6):632–5

Aström A, Pettersson U, Chambon P, Voorhees JJ. Retinoic acid induction of human cellular retinoic acid-binding protein-II gene transcription is mediated by retinoic acid receptor-retinoid X receptor heterodimers bound to one far upstream retinoic acid-responsive element with 5-base pair spacing. J. Biol. Chem. 1994;269(35):22334–9

Aström A, Pettersson U, Voorhees JJ. Structure of the human cellular retinoic acid-binding protein II gene. Early transcriptional regulation by retinoic acid. J. Biol. Chem. 1992;267(35):25251–5

Berth-Jones J, Todd G, Hutchinson PE, Thestrup-Pedersen K, Vanhoutte FP. Treatment of psoriasis with oral liarozole: a dose-ranging study. Br. J. Dermatol. 2000;143(6):1170–6

Bhushan M, Burden AD, McElhone K, James R, Vanhoutte FP, Griffiths CEM. Oral liarozole in the treatment of palmoplantar pustular psoriasis: A randomized, double-blind, placebo-controlled study. Br. J. Dermatol. 2001;145(4):546–53

Bolger AM, Lohse M, Usadel B. Trimmomatic: A flexible trimmer for Illumina sequence data. Bioinformatics. 2014;30(15):2114–20

Bovenschen HJ, Otero ME, Langewouters AMG, van Vlijmen-Willems IMJJ, van Rens DWA, Seyger MMB, et al. Oral retinoic acid metabolism blocking agent Rambazole for plaque psoriasis: an immunohistochemical study. Br. J. Dermatol. 2007;156(2):263–70

Casals M, Campoy A, Aspiolea F, Carrasco MA, Camps A. Successful treatment of linear Darier's disease with topical adapalene. J. Eur. Acad. Dermatol. Venereol. 2009;23(2):237–8

Chilcott RP, Dalton CH, Emmanuel AJ, Allen CE, Bradley ST. Transepidermal water loss does not correlate with skin barrier function in vitro. J. Invest. Dermatol. Elsevier Masson SAS; 2002;118(5):871–5 Available from: http://dx.doi.org/10.1046/j.1523-1747.2002.01760.x

Cooper SM, Burge SM. Darier's disease: epidemiology, pathophysiology, and management. Am. J. Clin. Dermatol. 2003;4(2):97–105

Dai J, Choo M-K, Park JM, Fisher DE. Topical ROR Inverse Agonists Suppress Inflammation in Mouse Models of Atopic Dermatitis and Acute Irritant Dermatitis. J. Invest. Dermatol. 2017;137(12):2523–31

Dawson AL, Dellavalle RP. Acne vulgaris. BMJ. 2013;346(6):f2634

Diaz P, Huang W, Keyari CM, Buttrick B, Price L, Guilloteau N, et al. Development and Characterization of Novel and Selective Inhibitors of Cytochrome P450 CYP26A1, the Human Liver Retinoic Acid Hydroxylase. J. Med. Chem. 2016;59(6):2579–95

Diaz P, Isoherranen N, Buttrick B, Guilloteau N. Specific Inhibitors of Cytochrome P450 26 Retinoic Acid Hydroxylase. United States: United States Patent Office; 2018.

Dicken CH, Bauer EA, Hazen PG, Krueger GG, Marks JG, McGuire JS, et al. Isotretinoin

treatment of Darier's disease. J. Am. Acad. Dermatol. 1982;6(4):721–6

Digiovanna JJ, Mauro T, Milstone LM, Schmuth M, Toro JR. Systemic retinoids in the management of ichthyoses and related skin types. Dermatol. Ther. 2013;26(1):26–38

Durinck S, Spellman PT, Birney E, Huber W. Mapping identifiers for the integration of genomic datasets with the R/Bioconductor package biomaRt. Nat. Protoc. 2009;4(8):1184–91

Eckert RL, Crish JF, Efimova T, Dashti SR, Deucher A, Bone F, et al. Regulation of involucrin gene expression. J. Invest. Dermatol. Elsevier Masson SAS; 2004;123(1):13–22 Available from: http://dx.doi.org/10.1111/j.0022-202X.2004.22723.x

Elias PM, Fritsch PO, Lampe M, Williams ML, Brown BE, Nemanic M, et al. Retinoid effects on epidermal structure, differentiation, and permeability. Lab. Investig. 1981;44(6):531–40

Fisher GJ, Reddy AP, Datta SC, Kang S, Yi JY, Chambon P, et al. All-trans retinoic acid induces cellular retinol-binding protein in human skin in vivo. J. Invest. Dermatol. 1995;105(1):80–6

Fisher GJ, Talwar HS, Xiao JH, Datta SC, Reddy AP, Gaub MP, et al. Immunological identification and functional quantitation of retinoic acid and retinoid X receptor proteins in human skin. J. Biol. Chem. 1994;269(32):20629–35

Fisher GJ, Voorhees JJ. Molecular mechanisms of retinoid actions in skin. Faseb J. 1996;10(9):1002–13

Fort-Lacoste L, Verscheure Y, Tisne-Versailles J, Navarro R. Comedolytic effect of topical retinaldehyde in the rhino mouse model. Dermatology. 1999;199(SUPPL. 1):33–5

Foti RS, Isoherranen N, Zelter A, Dickmann LJ, Buttrick BR, Diaz P, et al. Identification of Tazarotenic Acid as the First Xenobiotic Substrate of Human Retinoic Acid Hydroxylase CYP26A1 and CYP26B1. J. Pharmacol. Exp. Ther. 2016;357(2):281–92

Frankart A, Malaisse J, De Vuyst E, Minner F, de Rouvroit CL, Poumay Y. Epidermal morphogenesis during progressive in vitro 3D reconstruction at the air-liquid interface. Exp. Dermatol. 2012;21(11):871–5

Gendimenico GJ, Stim TB, Corbo M, Mezick JA, Janssen B. A Pleiotropic Response Is Induced in F9 Embryonal Carcinoma Cells and Rhino Mouse Skin by All-trans-Retinoic Acid, a RAR Agonist but Not by SR11237, a RXR-Selective Agonist. J. Invest. Dermatol. Elsevier Masson SAS; 1994;102(5):676–80

Giltaire S, Herphelin F, Frankart A, Hérin M, Stoppie P, Poumay Y. The CYP26 inhibitor R115866 potentiates the effects of all-trans retinoic acid on cultured human epidermal keratinocytes. Br. J. Dermatol. 2009;160(3):505–13

Griffiths CE, Elder JT, Bernard BA, Rossio P, Cromie MA, Finkel LJ, et al. Comparison of CD271 (adapalene) and all-trans retinoic acid in human skin: dissociation of epidermal effects and CRABP-II mRNA expression. J. Invest. Dermatol. 1993. p. 325–8

Kang S, Duell EA, Fisher GJ, Datta SC, Wang ZQ, Reddy AP, et al. Application of retinol to human skin in vivo induces epidermal hyperplasia and cellular retinoid binding proteins characteristic of retinoic acid but without measurable retinoic acid levels or irritation. J. Invest. Dermatol. Elsevier Masson SAS; 1995;105(4):549–56

Kang S, Duell EA, Kim KJ, Voorhees JJ. Liarozole inhibits human epidermal retinoic acid 4-

hydroxylase activity and differentially augments human skin responses to retinoic acid and retinol in vivo. J. Invest. Dermatol. 1996;107(2):183–7

Kim D, Langmead B, Salzberg SL. HISAT: a fast spliced aligner with low memory requirements. Nat. Methods. 2015;12(4):357–60

Kim B, Langmead B, Salzberg S. genome_tran [Internet]. 2017 [cited 2018 Jun 25]. Available from: ftp://ftp.ccb.jhu.edu/pub/infphilo/hisat2/data/grch38_tran.tar.gz

Kim D, Pertea M, Kim D, Pertea GM, Leek JT, Salzberg SL. Transcript-level expression analysis of RNA- seq experiments with HISAT , StringTie and Transcript-level expression analysis of RNA-seq experiments with HISAT , StringTie and Ballgown. Nat. Protoc. Nature Publishing Group; 2016;11(9):1650–67

Kligman LH, Kligman AM. The effect on rhino mouse skin of agents which influence keratinization and exfoliation. J. Invest. Dermatol. Elsevier Masson SAS; 1979;73(5 I):354–8

Krämer A, Green J, Pollard J, Tugendreich S. Causal analysis approaches in ingenuity pathway analysis. Bioinformatics. 2014;30(4):523–30

Kuijpers ALA, Van Pelt JPA, Bergers M, Boegheim PJ, Den Bakker JEN, Siegenthaler G, et al. The effects of oral liarozole on epidermal proliferation and differentiation in severe plaque psoriasis are comparable with those of acitretin. Br. J. Dermatol. 1998;139(3):380–9

Kurlandsky SB, Duell EA, Kang S, Voorhees JJ, Fisher GJ. Auto-regulation of retinoic acid biosynthesis through regulation of retinol esterification in human keratinocytes. J. Biol. Chem. 1996;271(26):15346–52

Kypriotou M, Huber M, Hohl D. The human epidermal differentiation complex: Cornified envelope precursors, S100 proteins and the “fused genes” family. Exp. Dermatol. 2012;21(9):643–9

Lalevée S, Anno YN, Chatagnon A, Samarut E, Poch O, Laudet V, et al. Genome-wide in silico identification of new conserved and functional retinoic acid receptor response elements (direct repeats separated by 5 bp). J. Biol. Chem. 2011;286(38):33322–34

Laursen KB, Kashyap V, Scandura J, Gudas LJ. An alternative retinoic acid-responsive Stra6 promoter regulated in response to retinol deficiency. J. Biol. Chem. 2015;290(7):4356–66

Van Der Leede BJM, Van Den Brink CE, Pijnappel WWM, Sonneveld E, Van Der Saag PT, Van Der Burg B. Autoinduction of retinoic acid metabolism to polar derivatives with decreased biological activity in retinoic acid-sensitive, but not in retinoic acid-resistant human breast cancer cells. J. Biol. Chem. 1997;272(29):17921–8

Li H, Handsaker B, Wysoker A, Fennell T, Ruan J, Homer N, et al. The Sequence Alignment/Map format and SAMtools. Bioinformatics. 2009;25(16):2078–9

Loudig O, Babichuk C, White J, Abu-Abed S, Mueller C, Petkovich M. Cytochrome P450RAI(CYP26) promoter: a distinct composite retinoic acid response element underlies the complex regulation of retinoic acid metabolism. Mol. Endocrinol. 2000;14(9):1483–97

Love M, Anders S, Huber W. Differential analysis of RNA-Seq data at the gene level using the DESeq package. 2013;1–32

Lucker GPH, Heremans AMC, Boegheim PJ, Van De Kerkhof PCM, Steijlen PM. Oral

treatment of ichthyosis by the cytochrome P-450 inhibitor liarozole. Br. J. Dermatol. 1997;136(1):71–5

Lucker GPH, Verfaille CJ, Heremans AMC, Vanhoutte FP, Boegheim JPJ, Steijlen PPM. Topical liarozole in ichthyosis: A double-blind, left-right comparative study followed by a long-term open maintenance study [2]. Br. J. Dermatol. 2005;152(3):566–9

Marikar Y, Wang Z, Petkovich M, Voorhees JJ, Fisher GJ, Duell EA. Retinoic Acid Receptors Regulate Expression of Retinoic Acid 4-Hydroxylase that Specifically Inactivates All-Trans Retinoic Acid in Human Keratinocyte HaCaT Cells. J. Invest. Dermatol. Elsevier Masson SAS; 1998;111(3):434–9

Mihály J, Gamlieli A, Worm M, Rühl R. Decreased retinoid concentration and retinoid signalling pathways in human atopic dermatitis. Exp. Dermatol. 2011;20(4):326–30

Minner F, Herphelin F, Poumay Y. Study of Epidermal Differentiation in Human Keratinocytes Cultured in Autocrine Conditions. Biol. Integument. 2010. p. 71–82

Monzon RI, LaPres JJ, Hudson LG. Regulation of involucrin gene expression by retinoic acid and glucocorticoids. Cell Growth Differ. 1996;7(12):1751–9

Nelson CH, Buttrick BR, Isoherranen N. Therapeutic potential of the inhibition of the retinoic acid hydroxylases CYP26A1 and CYP26B1 by xenobiotics. Curr. Top. Med. Chem. NIH Public Access; 2013;13(12):1402–28

Okano J, Lichti U, Mamiya S, Aronova M, Zhang G, Yuspa S, et al. Increased retinoic acid levels through ablation of Cyp26b1 determine the processes of embryonic skin barrier formation and peridermal development. J. Cell Sci. 2012;125(Pt 7):1827–36

Orfanos CE, Zouboulis CC, Almond-Roesler B, Geilen CC. Current use and future potential role of retinoids in dermatology. Drugs. 1997;53(3):358–88

Pavez Loriè E, Chamcheu JC, Vahlquist A, Törmä H. Both all-trans retinoic acid and cytochrome P450 (CYP26) inhibitors affect the expression of vitamin A metabolizing enzymes and retinoid biomarkers in organotypic epidermis. Arch. Dermatol. Res. Springer-Verlag; 2009a;301(7):475–85

Pavez Loriè E, Cools M, Borgers M, Wouters L, Shroot B, Hagforsen E, et al. Topical treatment with CYP26 inhibitor talarozole (R115866) dose dependently alters the expression of retinoid-regulated genes in normal human epidermis. Br. J. Dermatol. Blackwell Publishing Ltd; 2009b;160(1):26–36

Pertea M, Pertea GM, Antonescu CM, Chang TC, Mendell JT, Salzberg SL. StringTie enables improved reconstruction of a transcriptome from RNA-seq reads. Nat. Biotechnol. 2015;33(3):290–5

Poumay Y, Dupont F, Marcoux S, Leclercq-Smekens M, Hérin M, Coquette A. A simple reconstructed human epidermis: Preparation of the culture model and utilization in in vitro studies. Arch. Dermatol. Res. 2004;296(5):203–11

Poumay Y, Herphelin F, Smits P, De Potter IY, Pittelkow MR. High-cell-density phorbol Ester and retinoic acid upregulate involucrin and downregulate Suprabasal Keratin 10 in autocrine cultures of human epidermal keratinocytes. Mol. Cell Biol. Res. Commun. 1999;2(2):138–44

Radoja N, Diaz D V., Minars TJ, Freedberg IM, Blumenberg M, Tomic- Canic M. Specific organization of the negative response elements for retinoic acid and thyroid hormone receptors in keratin gene family. J. Invest. Dermatol. 1997;109(4):566–72

Ray WJ, Bain G, Yao M, Gottlieb DI. CYP26, a novel mammalian cytochrome P450, is induced by retinoic acid and defines a new family. J. Biol. Chem. 1997;272(30):18702–8

RCoreTeam. R: A Language and Environment for Statistical Computing [Internet]. Vienna, Austria; 2018. Available from: https://www.r-project.org

Rittié L, Varani J, Kang S, Voorhees JJ, Fisher GJ. Retinoid-induced epidermal hyperplasia is mediated by epidermal growth factor receptor activation via specific induction of its ligands heparin-binding EGF and amphiregulin in human skin in vivo. J. Invest. Dermatol. 2006;126(4):732–9

Schindelin J, Arganda-Carreras I, Frise E, Kaynig V, Longair M, Pietzsch T, et al. Fiji: an open-source platform for biological-image analysis. Nat. Methods. 2012;9(7):676–82

Seiberg M, Siock P, Wisniewski S, Cauwenbergh G, Shapiro SS. The effects of trypsin on apoptosis, utriculi size, and skin elasticity in the Rhino mouse. J. Invest. Dermatol. 1997;109(3):370–6

Stehlin-Gaon C, Willmann D, Zeyer D, Sanglier S, Van Dorsselaer A, Renaud JP, et al. All-trans retinoic acid is a ligand for the orphan nuclear receptor RORβ. Nat. Struct. Biol. 2003;10(10):820–5

Steijlen PM, Reifenschweiler DOH, Ramaekers FCS, van Muijen GNP, Happle R, Link M, et al. Topical treatment of ichthyoses and Darier's disease with 13-cis-retinoic acid - A clinical and immunohistochemical study. Arch. Dermatol. Res. 1993;285(4):221–6

Stoll SW, Elder JT. Retinoid regulation of heparin-binding EGF-like growth factor gene expression in human keratinocytes and skin. Exp. Dermatol. 1998;7(6):391–7

Stoppie P, Borgers M, Borghgraef P, Dillen L, Goossens J, Sanz G, et al. R115866 inhibits all-trans-retinoic acid metabolism and exerts retinoidal effects in rodents. J. Pharmacol. Exp. Ther. 2000;293(1):304–12

de Thé H, Vivanco-Ruiz MM, Tiollais P, Stunnenberg H, Dejean A. Identification of a retinoic acid responsive element in the retinoic acid receptor beta gene. Nature. 1990;343(6254):177–80

Tomic-Canic M, Sunjevaric I, Freedberg IM, Blumenberg M. Identification of the retinoic acid and thyroid hormone receptor-responsive element in the human K14 keratin gene. J. Invest. Dermatol. 1992;99(6):842–7

Vahlquist A, Blockhuys S, Steijlen P, Van Rossem K, Didona B, Blanco D, et al. Oral liarozole in the treatment of patients with moderate/severe lamellar ichthyosis: Results of a randomized, double-blind, multinational, placebo-controlled phase II/III trial. Br. J. Dermatol. 2014;170(1):173–81

Vahlquist A, Gånemo A, Virtanen M. Congenital ichthyosis: An overview of current and emerging therapies. Acta Derm. Venereol. 2008. p. 4–14

Vasios GW, Gold JD, Petkovich M, Chambon P, Gudas LJ. A retinoic acid-responsive element is present in the 5' flanking region of the laminin B1 gene. Proc Natl Acad Sci U S A.

1989;86(23):9099–103

Verfaille CJ, Borgers M, van Steensel MAM. Retinoic acid metabolism blocking agents (RAMBAs): a new paradigm in the treatment of hyperkeratotic disorders. J. der Dtsch. Dermatologischen Gesellschaft = J. Ger. Soc. Dermatology JDDG. 2008;6(5):355–64

Verfaille CJ, Thissen CACB, Bovenschen HJ, Mertens J, Steijlen PM, Van De Kerkhof PCM. Oral R115866 in the treatment of moderate to severe plaque-type psoriasis. J. Eur. Acad. Dermatology Venereol. 2007a;21(8):1038–46

Verfaille CJ, Vanhoutte FP, Blanchet-Bardon C, Van Steensel MA, Steijlen PM. Oral liarozole vs. acitretin in the treatment of ichthyosis: A phase II/III multicentre, double-blind, randomized, active-controlled study. Br. J. Dermatol. 2007b;156(5):965–73

De Vuyst E, Charlier C, Giltaire S, De Glas V, de Rouvroit CL, Poumay Y. Reconstruction of normal and pathological human epidermis on polycarbonate filter. Methods Mol. Biol. 2014;1195(1202):191–201

Van Wauwe J, Van Nyen G, Coene MC, Stoppie P, Cools W, Goossens J, et al. Liarozole, an inhibitor of retinoic acid metabolism, exerts retinoid-mimetic effects in vivo. J. Pharmacol. Exp. Ther. 1992;261(2):773–9

Willems E, Leyns L, Vandesompele J. Standardization of real-time PCR gene expression data from independent biological replicates. Anal. Biochem. 2008;379(1):127–9

Xiao JH, Feng X, Di W, Peng ZH, Li L a, Chambon P, et al. Identification of heparin-binding EGF-like growth factor as a target in intercellular regulation of epidermal basal cell growth by suprabasal retinoic acid receptors. EMBO J. 1999;18(6):1539–48

Yoshimura K, Uchida G, Okazaki M, Kitano Y, Harii K. Differential expression of heparin-binding EGF-like growth factor (HB-EGF) mRNA in normal human keratinocytes induced by a variety of natural and synthetic retinoids. Exp. Dermatol. Munksgaard International Publishers; 2003;12 Suppl 2(s2):28–34

Zheng D, Giljohann DA, Chen DL, Massich MD, Wang X-Q, Iordanov H, et al. Topical delivery of siRNA-based spherical nucleic acid nanoparticle conjugates for gene regulation. Proc. Natl. Acad. Sci. 2012;109(30):11975–80

Zhu A, Ibrahim JG, Love MI. Heavy-tailed prior distributions for sequence count data: removing the noise and preserving large differences. Bioinformatics. 2018;(November):1–9

FIGURE LEGENDS

Figure 1: DX314 potentiates a*t*RA gene expression effects in healthy RHE. (a) Relative expression of HBEGF, IVL, and CYP26A1 mRNA by RT-qPCR. Symbol underneath indicates comparison group (n=3-4 times in duplicate; mean±95% CI; *p≤0.05, **p≤0.01, ***p≤0.001; one-way ANOVA with Tukey's correction; *vs Control, †vs 1nM a*t*RA, ¥vs 10nM a*t*RA, ⊗vs DX314-alone, ⊕vs Liarozole-alone). **(b)** IVL localization in healthy RHE. **(c)** RNAseq: Relative mRNA expression of retinoid-responsive genes in healthy RHE. Non-grey cells differ from controls (FDR≤0.05; n=3-5). Adjacent green cell indicates likely RAR-mediated effect based on presence of RARE-promotor for respective gene. Predicted activation z-score of **(d)** upstream regulators or **(e)** canonical pathways determined by IPA software utilizing RNAseq data. Black dots indicate statistical insignificance (p≤0.05 and z-score ≥2 or ≤-2). Additional abbreviations: **Table S4**.

Figure 2: DX314 potentiates the effects of a*t*RA on CYP26A1 mRNA expression in keratinocytes from individuals with keratinization disorders. Relative CYP26A1 mRNA expression by RT-qPCR in; **(a)** Darier disease RHE, **(b)** recessive x-linked ichthyosis (RXLI) full-thickness RHE, **(c)** lamellar ichthyosis RHE, and **(d)** RXLI monolayer keratinocyte cultures. RHE were treated for 4 days and monolayer keratinocytes for 20hrs. Statistical significance was computed with **(a)** autoscaled or **(b-d)** raw dCt values. Symbol below each treatment indicates comparison group (n=3 independent replicates with technical duplicates; mean±95% CI; *p≤0.05; **p≤0.01; ***p≤0.001; one-way ANOVA with Tukey's correction; *vs Control, †vs 1nM a*t*RA, ¥vs 10nM a*t*RA, &vs 100nM a*t*RA, ◆vs 1000nM a*t*RA, ⊗vs DX314-alone, ⊕vs Liarozole-alone, ∅vs Talarozole-alone).

Figure 3: DX314 potentiates the effects of a*t*RA on the expression and localization of keratin 10 (KRT10) in Darier disease (DD) RHE. A*t*RA, but not DX314, induces a loss of stratum granulosum. (a) HE staining and **(b)** immunofluorecent staining of KRT10 (green) localization with nuclear stain (blue), in DD RHE treated for 4 days. Scale bars: black = 20µm, white =50 µm. **(c)** Relative KRT10 mRNA expression by qPCR. Symbol below each treatment indicates comparison group. (n=3 independent replicates with technical duplicates; mean±95% CI; *p≤0.05; **p≤0.01; ***p≤0.001; one-way ANOVA with Tukey's correction on autoscaled values; *vs Control, †vs 1nM a*t*RA, ¥vs 10nM a*t*RA, &vs 100nM a*t*RA, ⊗vs DX314-alone, ø vs Talarozole-alone).

Figure 4: DX314 protects barrier function in RHE. (a) Transepithelial electrical resistance (TEER) in healthy RHE. TEER was normalized to control RHEs for each run, then pooled for analysis. Graph shows Tukey's boxplot with outliers. Sample sizes (n) are shown above x-axis. **(b)** LI RHE TEER (top), transepidermal water loss (middle), and the linear correlation between the two measures (bottom). **(c)** HE staining of lamellar ichthyosis (LI) RHE. Scale bar = 50µm. **(d)** Semi-quantitative analysis of relative stratum granulosum (SG) surface area in healthy RHE. **(e)** Relative expression of epidermal differentiation complex (EDC) genes and regulators by RNAseq. Colored (non-grey) cells indicate statistical significance from control (FDR≤0.05; n=3-5). All RHE received a 4-day treatment. **(a,b,d)** (*p≤0.05; **p≤0.01; ***p≤0.001; one-way ANOVA with Dunnett's correction vs control).

Figure 5: DX314 reduces rhino mouse skin abnormalities. Representative HE staining of skin biopsies from rhino mice topically treated for 11 days with vehicle (acetone) or 1% DX314. ImageJ software was used to quantify comedonal number, profile (d/D, ratio of opening to inner diameter), and epidermal thickness. Epidermal thickness was measured at multiple points across each sample by measuring the sum of epidermal areas (yellow), excluding the corneal layer, and dividing by the sum of the length of the basal layers (dotted blue line). Scale bar =200µm.

Figure 6: DX314 treatment reduces comedonal number, induces epidermal thickening, and increases comedonal profile, while having no effect on transepidermal water loss (TEWL) in treated rhino mice. Semi-quantitative analysis of changes in **(a)** total (open + closed) and **(b)** open comedonal number, **(c)** comedonal profile, and **(d)** epidermal thickness in rhino mice topically treated with vehicle (acetone) or 1% DX314 over 11 days. **(e)** Daily TEWL measurements did not reveal any statistically significant differences between treatment groups. (n=5-6 mice per treatment; mean±SD; *p≤0.05; **p≤0.01; Student's t-test vs vehicle control).

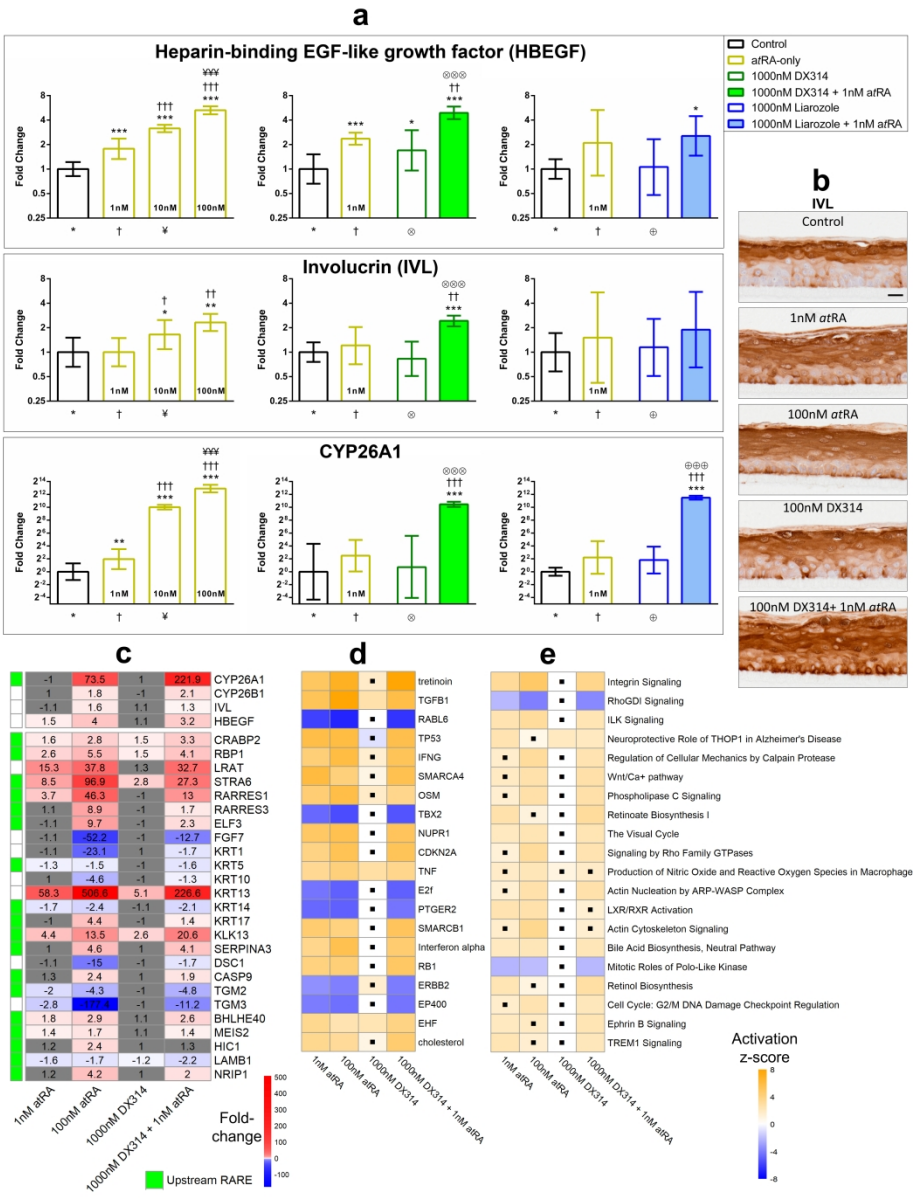

Figure 1: DX314 potentiates a*t*RA gene expression effects in healthy RHE. (a) Relative expression of HBEGF, IVL, and CYP26A1 mRNA by RT-qPCR. Symbol underneath indicates comparison group (n=3-4 times in duplicate; mean±95% CI; *p≤0.05, **p≤0.01, ***p≤0.001; one-way ANOVA with Tukey's correction; *vs Control, †vs 1nM a*t*RA, $^{¥}$vs 10nM a*t*RA, $^{\otimes}$vs DX314-alone, $^{\oplus}$vs Liarozole-alone). **(b)** IVL localization in healthy RHE. **(c)** RNAseq: Relative mRNA expression of retinoid-responsive genes in healthy RHE. Non-grey cells differ from controls (FDR≤0.05; n=3-5). Adjacent green cell indicates likely RAR-mediated effect based on presence of RARE-promotor for respective gene. Predicted activation z-score of **(d)** upstream regulators or **(e)** canonical pathways determined by IPA software utilizing RNAseq data. Black dots indicate statistical insignificance (p≤0.05 and z-score ≥2 or ≤-2). Additional abbreviations: **Table S4**.

190x249mm (600 x 600 DPI)

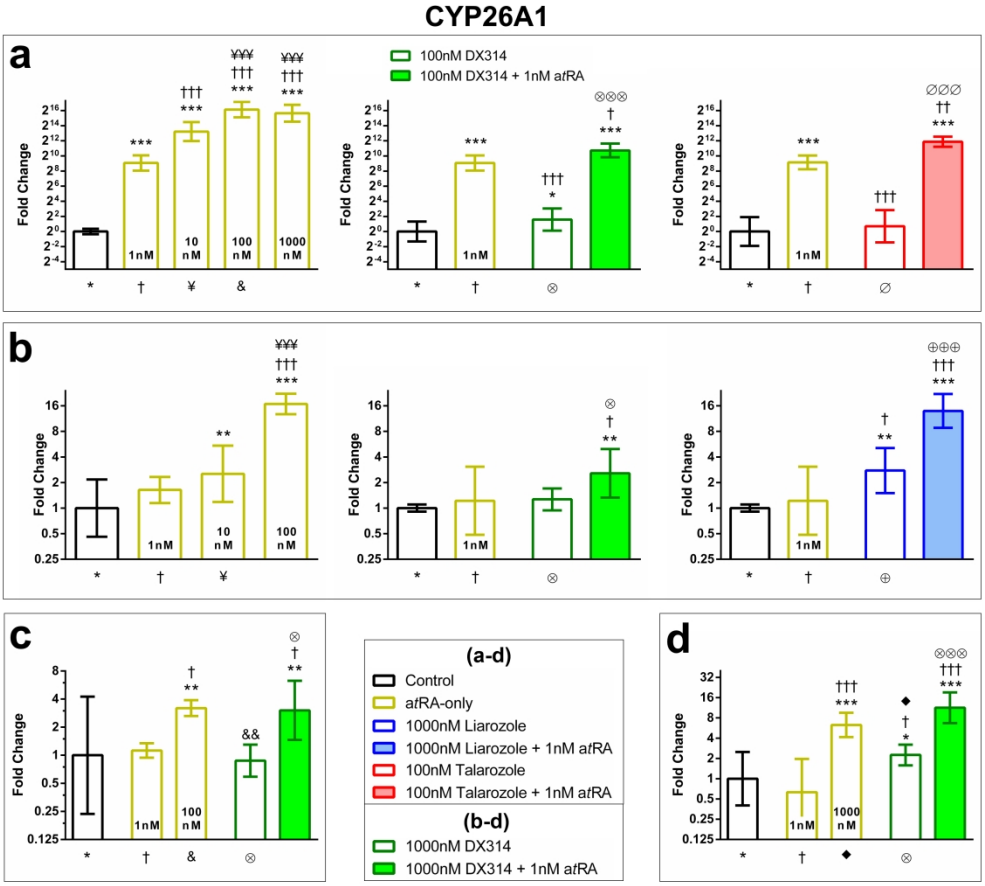

Figure 2: DX314 potentiates the effects of *at*RA on CYP26A1 mRNA expression in keratinocytes from individuals with keratinization disorders. Relative CYP26A1 mRNA expression by RT-qPCR in; **(a)** Darier disease RHE, **(b)** recessive x-linked ichthyosis (RXLI) full-thickness RHE, **(c)** lamellar ichthyosis RHE, and **(d)** RXLI monolayer keratinocyte cultures. RHE were treated for 4 days and monolayer keratinocytes for 20hrs. Statistical significance was computed with **(a)** autoscaled or **(b-d)** raw dCt values. Symbol below each treatment indicates comparison group (n=3 independent replicates with technical duplicates; mean±95% CI; *p≤0.05; **p≤0.01; ***p≤0.001; one-way ANOVA with Tukey's correction; *vs Control, †vs 1nM *at*RA, $^{¥}$vs 10nM *at*RA, $^{\&}$vs 100nM *at*RA, $^{\blacklozenge}$vs 1000nM *at*RA, $^{\otimes}$vs DX314-alone, $^{\oplus}$vs Liarozole-alone, $^{\varnothing}$vs Talarozole-alone).

150x135mm (600 x 600 DPI)

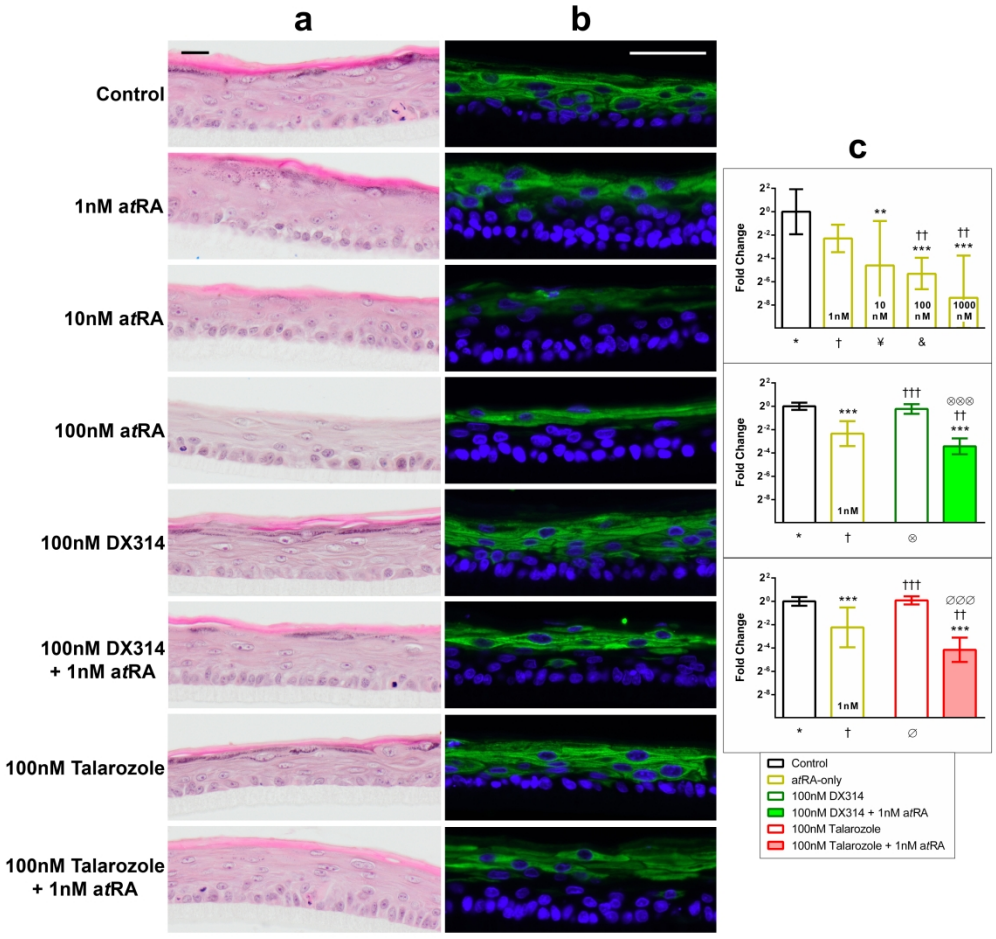

Figure 3: DX314 potentiates the effects of *at*RA on the expression and localization of keratin 10 (KRT10) in Darier disease (DD) RHE. A*t*RA, but not DX314, induces a loss of stratum granulosum. **(a)** HE staining and **(b)** immunofluorecent staining of KRT10 (green) localization with nuclear stain (blue), in DD RHE treated for 4 days. Scale bars: black = 20μm, white =50 μm. **(c)** Relative KRT10 mRNA expression by qPCR. Symbol below each treatment indicates comparison group. (n=3 independent replicates with technical duplicates; mean±95% CI; *p≤0.05; **p≤0.01; ***p≤0.001; one-way ANOVA with Tukey's correction on autoscaled values; *vs Control, †vs 1nM a*t*RA, $^{¥}$vs 10nM a*t*RA, $^{\&}$vs 100nM a*t*RA, $^{\otimes}$vs DX314-alone, $^{\emptyset}$vs Talarozole-alone).

182x171mm (600 x 600 DPI)

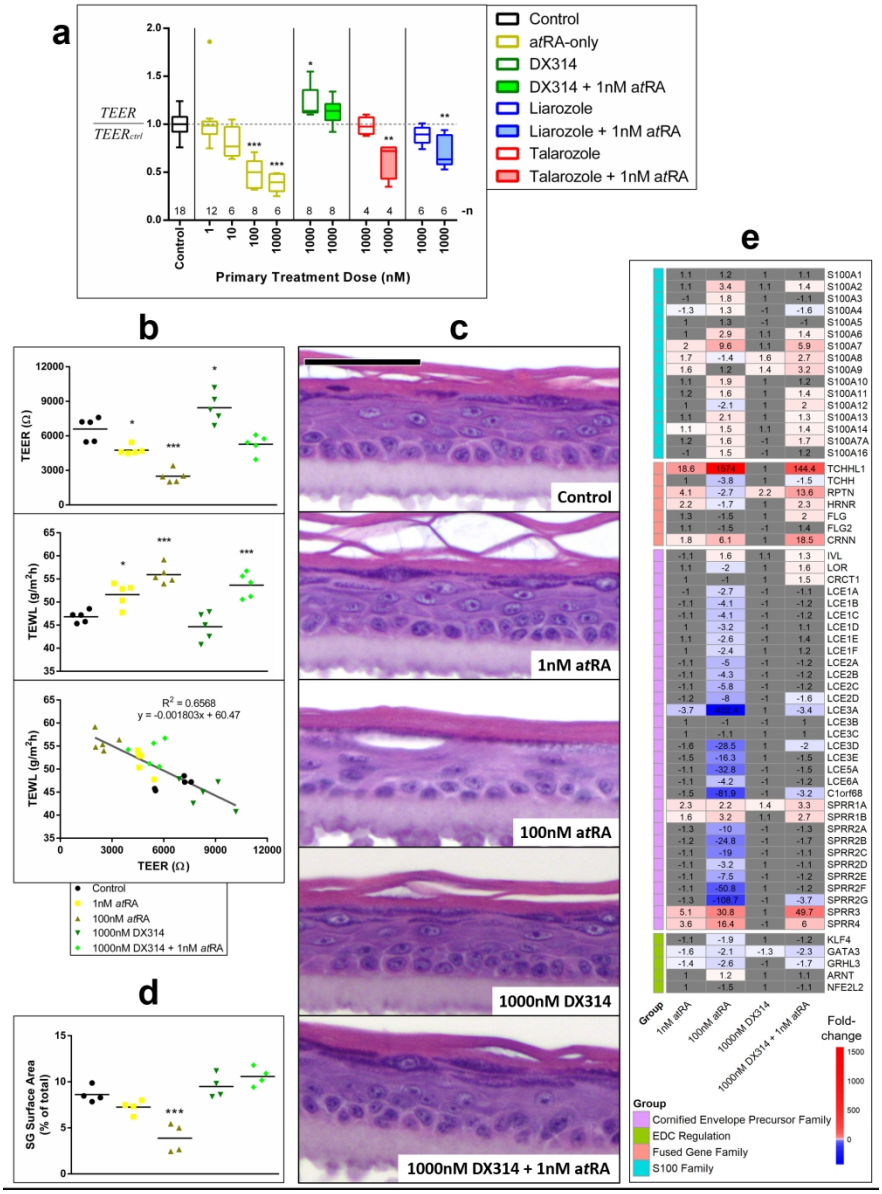

Figure 4: DX314 protects barrier function in RHE. (a) Transepithelial electrical resistance (TEER) in healthy RHE. TEER was normalized to control RHEs for each run, then pooled for analysis. Graph shows Tukey's boxplot with outliers. Sample sizes (n) are shown above x-axis. **(b)** LI RHE TEER (top), transepidermal water loss (middle), and the linear correlation between the two measures (bottom). **(c)** HE staining of lamellar ichthyosis (LI) RHE. Scale bar = 50μm. **(d)** Semi-quantitative analysis of relative stratum granulosum (SG) surface area in healthy RHE. **(e)** Relative expression of epidermal differentiation complex (EDC) genes and regulators by RNAseq. Colored (non-grey) cells indicate statistical significance from control (FDR≤0.05; n=3-5). All RHE received a 4-day treatment. **(a,b,d)** (*p≤0.05; **p≤0.01; ***p≤0.001; one-way ANOVA with Dunnett's correction vs control).

86x119mm (600 x 600 DPI)

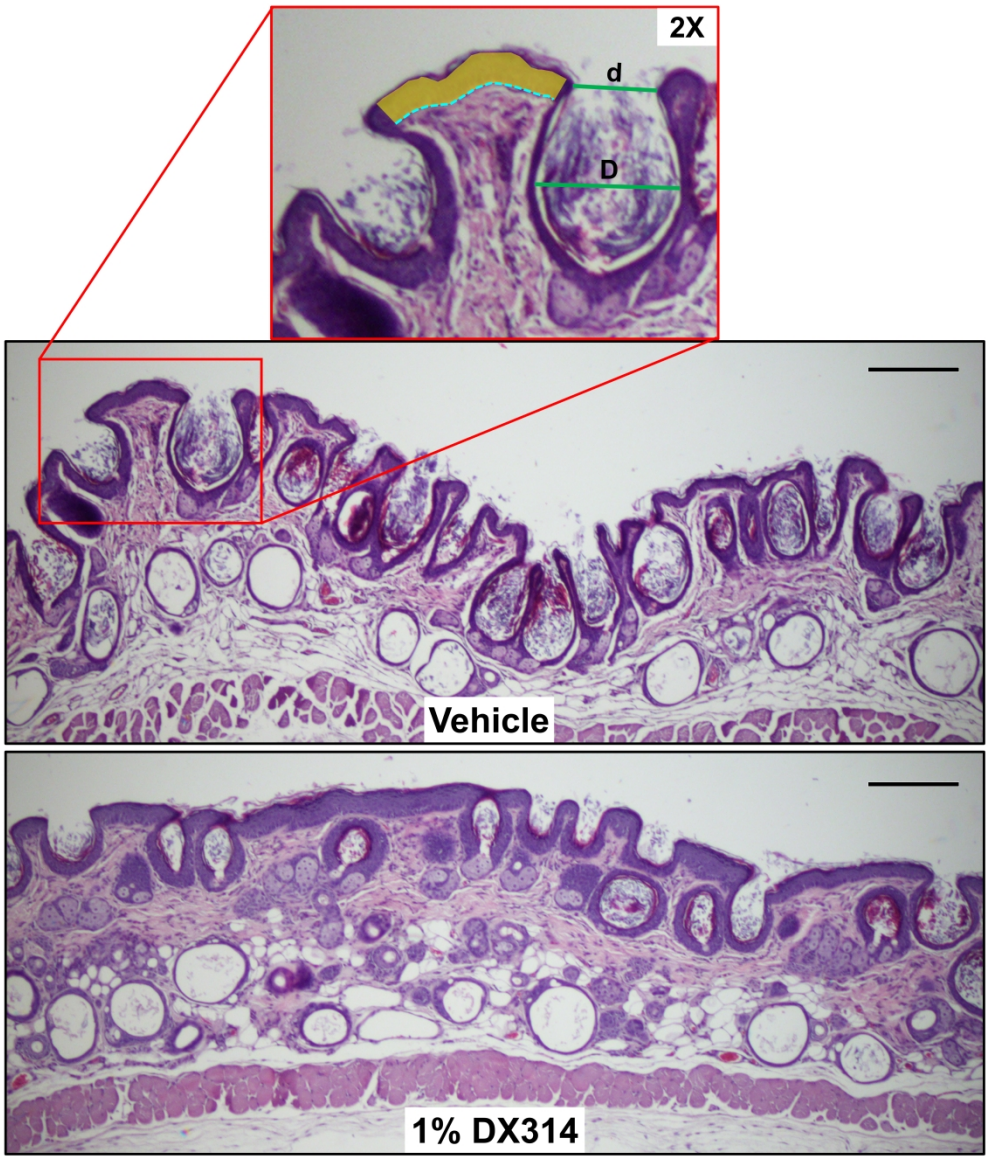

Figure 5: DX314 reduces rhino mouse skin abnormalities. Representative HE staining of skin biopsies from rhino mice topically treated for 11 days with vehicle (acetone) or 1% DX314. ImageJ software was used to quantify comedonal number, profile (d/D, ratio of opening to inner diameter), and epidermal thickness. Epidermal thickness was measured at multiple points across each sample by measuring the sum of epidermal areas (yellow), excluding the corneal layer, and dividing by the sum of the length of the basal layers (dotted blue line). Scale bar =200μm.

221x256mm (600 x 600 DPI)

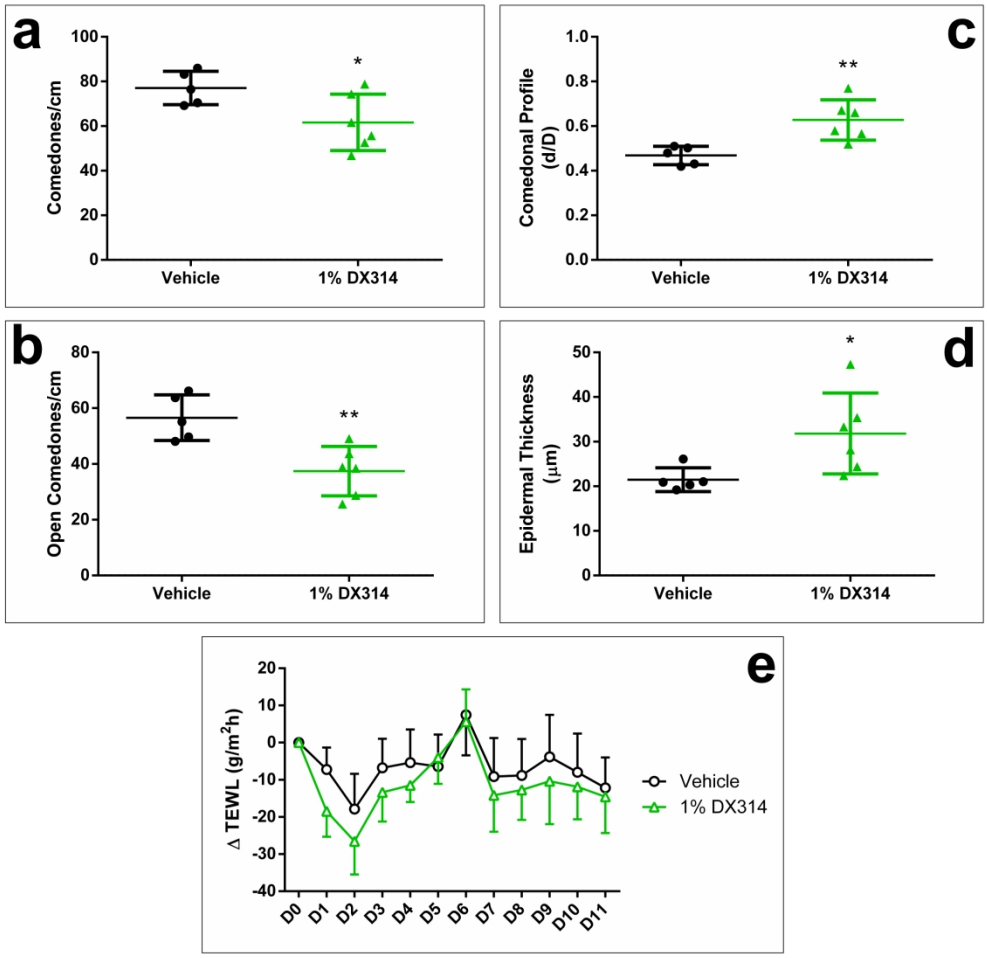

Figure 6: DX314 treatment reduces comedonal number, induces epidermal thickening, and increases comedonal profile, while having no effect on transepidermal water loss (TEWL) in treated rhino mice. Semi-quantitative analysis of changes in **(a)** total (open + closed) and **(b)** open comedonal number, **(c)** comedonal profile, and **(d)** epidermal thickness in rhino mice topically treated with vehicle (acetone) or 1% DX314 over 11 days. **(e)** Daily TEWL measurements did not reveal any statistically significant differences between treatment groups. (n=5-6 mice per treatment; mean±SD; *p≤0.05; **p≤0.01; Student's t-test vs vehicle control).

113x110mm (600 x 600 DPI)

SUPPLEMENTARY METHODS

Immunostaining

Slides were sequentially exposed to the following: PBS rinse, 2x 3min 0.1M glycine in dH2O, PBS rinse, then 1hr in PBS/BSA/Triton (PBS with 0.2% BSA and 0.02% Triton X-100). A hydrophobic marker was used to encircle the tissue and 50µL of primary antibody (diluted in PBS/BSA/Triton) was applied. The slides were placed in a humidity chamber and incubated for 1hr at room temperature. The slides were then rinsed three times in PBS/BSA/Triton before 1hr humidified incubation with 50µL of the respective secondary antibody. The slides were again rinsed three times in PBS/BSA/Triton before a 15min incubation with 50µL of Hoechst nuclear stain (diluted in PBS/BSA/Triton) followed by 3x 5min PBS rinses. Coverslips were mounted with Mowiol 40-88 and the slides were stored at 4°C until imaged on an Olympus DX63 microscope with Olympus XM10 camera. Antibodies and dilutions can be found below (**Table S3**).

RNA isolation and quantitative PCR

Following treatment, RHEs intended for RNA extraction were flash frozen at -80°C until use. RNA was isolated using the NucleoSpin RNA (Macherey-Nagel, Bethlehem, PA) kit, as recommended by the manufacturer. Variations from the standard protocol include homogenization with 600µL (rather than 350µL) of RA1 lysis buffer, addition of 6µL of β-mercaptoethanol to RA1 to aid tissue lysis, and addition 600µL of 70% ethanol (rather than 350µL) during nucleic acid precipitation. RNA obtained from monolayer and full-thickness RHE cultures were isolated using TRIzol (Life Technologies, Burlington, Canada) phenol-chloroform extraction as described by the manufacturer. Variations from the standard protocol include chilling the sample following the addition of isopropanol to encourage nucleic acid precipitation,

and the addition of a second chilled 75% ethanol wash prior to drying the pellet, which greatly improved consistency in RNA purity.

Isolated RNA purity and concentration were measured by NanoDrop 2000c (Thermo Scientific, Rockford, IL) and integrity was confirmed by gel electrophoresis. 100-200ng of template RNA was reverse-transcribed to cDNA with the Superscript III reverse transcriptase kit (Invitrogen, Aalst, Belgium). The cDNA was then diluted 1:10 with water. 2µL of cDNA was added to a 10µL real-time qPCR reaction, which used Takyon No ROX SYBR 2X MasterMix (Eurogentec, Seraing, Belgium) on a Roche Lightcycler 96 (activation: 3min - 95°C; 40 cycles: 10sec - 95°C, 20sec - 60°C, 30sec - 72°C). 500nM of each primer pair (**Table S2**), optimized for an annealing temperature of 60°C, was used for each reaction. RPL13a and 36B4 (RPLP0) were used as reference genes.

RNA sequencing and bioinformatics

RNA samples were sent to the University of Colorado's Genomics and Sequencing Core Facility (Denver, CO) for library preparation and sequencing. Purity and concentration were measured with an Agilent Bioanalyzer (Agilent Technologies, Santa Clara, CA). 200-500ng of RNA was used to prepare the Illumina HiSeq libraries according to manufacturer's instructions for the TruSeq Stranded RNA kit (Illumina, San Diego, CA). Sequencing was done as 2x151bp paired end reads on the Illumina HiSeq4000. The bioinformatics pipeline used was an adaptation of several described methods (Kim et al. 2016; Love et al. 2013): FastQC (Andrews 2010) (v0.11.3) → Trimmomatic (Bolger et al. 2014) (v0.38) → FastQC → Hisat2 (Kim et al. 2015) (v2.1.0) → SamTools (Li et al. 2009) (v1.8) → Stringtie (Pertea et al. 2015) (v1.3.4d). Reads were mapped to the H. sapien GRCh38 *genome_tran* index provided by HiSat2 developers (Kim et al. 2017). Differential expression analysis was performed in R (RCoreTeam 2018) (v3.5.2)

using DESeq2 (Love et al. 2014) (v1.22.2). False-discovery rate (FDR) was determined with the Benjamini-Hochberg correction, logarithmic-fold change shrinkage to correction was performed using the apeglm (Zhu et al. 2018) (v1.4.2) algorithm, HGNC names were attached using BiomaRt (Durinck et al. 2009) (v2.38.0). Treatment groups: Control (n=5), 1nM *at*RA (n=4), 100nM *at*RA (n=4), 1000nM DX314 (n=3), and 1000nM DX314 + 1nM *at*RA (n=4).

Fold-change (FC) and FDR values mapped to Ensembl IDs were imported into Ingenuity Pathway Analysis (IPA) (Qiagen, Germantown, MD) software for analysis. Analysis was limited to genes with FDR ≤ 0.05, and FC ≥ 1.5 or ≤ -1.5. IPA uses Fisher's exact test ($p \leq 0.05$) to predict the activation or inhibition of canonical pathways and upstream regulators. A z-score of ≥ 2.0 is considered activated, a z≤ -2.0 is considered inhibited.

Nuclear receptor profiling

Nuclear receptor activity profiling was performed by luciferase gene reporter assay using the Steady-Glo luciferase assay system (Promega, E2550) and 16 recombinant HeLa cell lines in which the respective human nuclear receptors were overexpressed. Compounds were solubilized at 10mM in DMSO and all assays were performed at a final concentration of 0.1% DMSO. Dose-response curves were generated with 8 compound concentrations (n=2) in 4-fold serial dilutions from a maximum test dose of 10µM. Cells in growth media (DMEM with 1g/L glucose (Invitrogen, 31885-023), 2mM L-glutamine (Invitrogen, 25030-024), 1x MEM non-essential amino acids (Invitrogen, 11140-035), 0.1% antibiotic-antimycotic (Invitrogen, 15240-062), 0.5mg/mL G418 (Invitrogen, 10131-027), 0.5µg/mL puromycin (Sigma, P8833), 10% FBS (Biowest, S800)) were seeded in 96-well plates at 2e4 cells/well and incubated at 37°C with 5% CO_2 for 4hrs. Compounds in test media (growth media with 0.1% Pluronic F-127 (Interchim, FP-379951)) were then added to each well and the plates were returned to the incubator for 18-

24hrs. 50µL/well of Steady-Glo was added to each well and plates were shaken for 5min at room temperature before measuring luciferase activity (RLU) using a BMG Clariostar plate reader.

Data was normalized to negative (Min) and positive (Max) controls: $\frac{(x-Min)*100}{(Max-Min)}$. 4-parameter logistic model fitting was performed using XLfit software (IDBS). Where n is the hill coefficient: $Normalized\ Activation\ (\%) = Min + \frac{(Max-Min)}{1+(EC50/x)^{n}}$.

Rhino mice

Rhino mice (2-3 males, 3 females per group), aged 5-7 weeks were acquired from Jackson Laboratory (Sacramento, CA) and acclimated to standard housing and provisions for one week prior to start. All animal studies were approved by Institutional Animal Care and Use Committee under NIH guidelines. Mice received daily topical application of 50µL vehicle (acetone), or freshly made 1% DX314, on a 2x2cm area of back skin for 11 days. Daily clinical observations, body weights, TEWL, and DRAIZE scoring were recorded (**Table S5** and **S6**). Mice underwent necropsy on day 12 and skin tissue was collected and processed.

Quantitative analysis of the tissue was performed using Fiji/ImageJ software following a previously described standardized method (Bouclier et al. 1991). Each sample was analyzed at least two different section depths and totaling 6.2-12.8mm of skin per subject. Open comedone profile was quantified as the ratio of the opening size (d) and the internal diameter (D). Epidermal thickness was measured (17+ unique points per subject) by measuring the epidermal area, excluding the SC, and dividing by the length of the underlying basal layer (**Figure 5**).

Keratinocytes	Source	Pathology	Age/Sex	Figure(s)
NAK209	Poumay/Bienfait	Healthy	48/F	1a-b, 4a
NAK219			37/M	1a, 4a
NAK214			32/F	1a, 4a, S1, S2
HEKa	Gibco, C0055C		40/F	1c-e, 4d-e, S3
DARK1	Poumay/Bienfait	Darier disease	Child/M	2a, 3a-c
RXLI1653	Paller	Recessive x-linked ichthyosis	13/M	2b
RXLI1658			29/M	2d
LI173		Lamellar ichthyosis	9/M	2c, 4b-c

Target	Forward	Reverse
36B4	ATCAACGGGTACAAACGAGTC	CAGATGGATCAGCCAAGAAGG
RPL13a	CTCAAGGTCGTGCGTCTGAA	TGGCTGTCACTGCCTGGTACT
HBEGF	TGGCCCTCCACTCCTCATC	GGGTCACAGAACCATCCTAGCT
IVL	TGAAACAGCCAACTCCAC	TTCCTCTTGCTTTGATGGG
KRT10	ATCGATGACCTTAAAAATCAGATTCTC	GCAGAGCTACCTCATTCTCATAC
CYP26A1	GGGAGAGCGGCTGGACAT	TCCAAAGAGGAGTTCGGTTGA
CYP26B1	CCGCTTCCATTACCTCCCGTTC	CCACCGCCAGCACCTTCAG

Target	Species	Dilution	Source
IVL	Mouse	1:200	Invitrogen, I9018
KRT10	Mouse	1:100	DAKO, M7002
2°, HRP-conjugated (anti-mouse)	Horse	1:100	Vectastain, PK-4002
2°, Alexa Fluor 488-conjugated (anti-mouse)	Goat	1:1000	Life Technologies, A11001
Hoechst 33258, nuclear stain	-	1:100	Life Technologies, H3569

AD	atopic dermatitis
ANOVA	analysis of variance
AQP	aquaporin
ARNT	aryl hydrocarbon receptor nuclear translocator
ARP	actin-related protein
***at*RA**	all-trans retinoic acid
BHLH	basic helix-loop-helix
C1orf	chromosome 1 open reading frame
CASP	caspase
CE	cornified envelope
CLDN	claudin
CRABP	cellular retinoic acid binding protein
CRBP	cellular retinol binding protein
CRCT	cysteine rich C-terminal
CRNN	cornulin
CYP	cytochrome P450
DD	Darier disease
DMSO	dimethyl sulfoxide
DNA	deoxyribonucleic acid
DSC	desmocollin
ECM	extracellular matrix
EDC	epidermal differentiation complex
EDTA	ethylenediaminetetraacetic acid
EGF	epidermal growth factor
EHF	ETS homologous factor
ELF	E74 like ETS transcription factor
ERBB	Erb-B2 Receptor Tyrosine Kinase
Erk	extracellular signal-regulated kinases
FBS	fetal bovine serum
FDR	false discovery rate
FGF	fibroblast growth factor
FLG	filaggrin
GATA	GATA binding protein
GRHL	grainyhead like transcription factor
GTF	gene transfer format
HBEGF	heparin-binding EGF-like growth factor
HE	hematoxylin and eosin
HGNC	HUGO gene nomenclature committee
HIC	HIC ZBTB transcriptional repressor
HKGS	human keratinocyte growth supplement
HRNR	hornerin
IF	immunofluorescence
IFNG	interferon gamma
IHC	immunohistochemistry
IL	interleukin
ILK	integrin-linked kinase
IPA	ingenuity pathway analysis
IVL	involucrin
JAK/STAT	janus kinases/signal transducer and activator of transcription

JAM	junctional adhesion molecules
KG	keratohyalin granules
KGF	keratinocyte growth factor
KLF	kruppel-like factor
KLK	kallikrein related peptidase
KRT	keratin
LAMB	laminin subunit beta
LCE	late cornified envelope
LI	lamellar ichthyosis
LOR	loricrin
LRAT	lecithin:retinol acetyltransferase
LXR	liver X receptor
MAPK	mitogen-activated protein kinases
MEIS	Meis homeobox
ML	Monolayer
NFE	nuclear factor, erythroid
NR	nuclear receptor
NRIP	nuclear receptor interacting protein
OCLN	occludin
OR	organotypic raft
P/S	penicillin/streptomycin
PBS	phosphate buffered saline
PKC	protein kinase C
PPAR	peroxisome-proliferator-activated receptor
RA	retinoic acid
RABL	rab-like protein
RAL	retinal
RalDH	retinal dehydrogenase
RAMBA	retinoic acid metabolism blocking agents
RAR	retinoic acid receptor
RARE	retinoic acid response element
RARRES	retinoic acid receptor responder
RB1	retinoblastoma-associated protein
RBP	retinol binding protein
RE	retinyl esters
RHE	reconstructed human epidermis
RHOGDI	RHO protein GDP dissociation inhibitor
RNA	ribonucleic acid
ROL	retinol/vitamin A
ROR	RAR-related orphan receptor
RPTN	repetin
RT qPCR	real-time quantitative polymerase chain reaction
RXLI	recessive x-linked ichthyosis
RXR	retinoid X receptor
S100	S100 calcium binding protein
SAM	sequence alignment map
SB	stratum basale
SC	stratum corneum
SDR	short-chain dehydrogenases/reductases

SG	stratum granulosum
SMARC	SWI/SNF-related matrix-associated actin-dependent regulator of chromatin
SPINK	serine protease inhibitor kazal-type
SPR	small proline-rich protein
SS	stratum spinosum
SSWL	subsurface water loss
STRA	stimulated by retinoic acid
TCHH/THH	trichohyalin
TEER	transepithelial electrical resistance
TEWL	trans-epidermal water loss
TGF	transforming growth factor
TGM	transglutaminases
THOP	thimet oligopeptidase
TJ	tight junction
TLR	toll-like receptor
TNF	tumor necrosis factor
TP53	tumor protein p53
TR	thyroid receptor
TREM	triggering receptor expressed on myeloid cells
TTR	transthyretine
UV	ultraviolet
VDR	vitamin D receptor
WASP	Wiskott–Aldrich Syndrome protein
Wnt	wingless/integrated
ZO	zona occludens

Group	Animal Number	Clinical Observation (Days Observed)
Vehicle	**101***	NSO (Day 0-5), slight dry skin on upper back (Day 6), dry skin on upper back (Day 7-8), slight dry skin on upper back (Day 9-11) NSO Day 12)
	102*	NSO (Day 0-8), very slight dry skin on upper back (Day 9), NSO (Day 10-12)
	103*	NSO (Day 0-5), slight dry skin on upper back (Day6-7), NSO (Day 8), two small bite marks at base of tail (Day 9-11), NSO (Day 12)
	152^	NSO (Day 0-6), Slight dry skin on upper back (Day 7-8), NSO (Day 9), Slight dry skin on upper back (Day 10-11), NSO (Day 12)
	153^	NSO (Day 0-7), Slight dry skin on upper back (Day 8), NSO (Day 9-12)
1% DX314	**401***	NSO (Day 0-5), Slight dry skin on upper back (Day 6-8), brown/tan patch across mid back (Day 9-12)
	402*	NSO (Day 0-6), Dry skin on upper back (Day 7), Slight dry skin on upper back (Day 8), Brown/tan patch across mid back (Day 9-12)
	403*	NSO (Day 0-6), Dry skin on upper back (Day 7), Slight dry skin on upper back (Day 8), Darker brown/tan patch across mid back (Day 9-12)
	451^	NSO (Day 0-6), slight dry skin on upper back (Day 7-8), NSO (Day 9-11), slight tan patch on mid back (Day 12)
	452^	NSO (Day 0-6), Slight dry skin on upper back (Day 7-8), NSO (Day 9-12)
	453^	NSO (Day 0-6), Slight dry skin on upper back (Day 7-8), NSO (Day 9-11), OD: corneal edema, swollen and opaque; tan patch on back (Day 12)

Group	Animal	Weight						DRAIZE Scoring (Erythema : Edema)		
		Day 0		Day 7		Day 12				
		g	%	g	%	g	%	Day 0	Day 7	Day 12
Vehicle	**101***	24.5	100.0	20.8	84.9	21.9	89.4	0 : 0	0 : 0	0 : 0
	102*	24.4	100.0	25.9	106.1	25.2	103.3	0 : 0	0 : 0	0 : 0
	103*	18.5	100.0	19.1	103.2	19.8	107.0	0 : 0	0 : 0	0 : 0
	152^	19.3	100.0	19.6	101.6	19.7	102.1	0 : 0	0 : 0	0 : 0
	153^	21.9	100.0	21.8	99.5	23.2	105.9	0 : 0	0 : 0	0 : 0
1% DX314	**401***	23.4	100.0	23.1	98.7	23.8	101.7	0 : 0	0 : 0	0 : 0
	404*	22.6	100.0	23.2	102.7	23.4	103.5	0 : 0	0 : 0	0 : 0
	403*	21.9	100.0	22.8	104.1	23.2	105.9	0 : 0	0 : 0	0 : 0
	451^	19.1	100.0	19.7	103.1	20.5	107.3	0 : 0	0 : 0	0 : 0
	452^	21.4	100.0	22.4	104.7	22.3	104.2	0 : 0	0 : 0	0 : 0
	453^	20.6	100.0	20.7	100.5	21.4	103.9	0 : 0	0 : 0	0 : 0

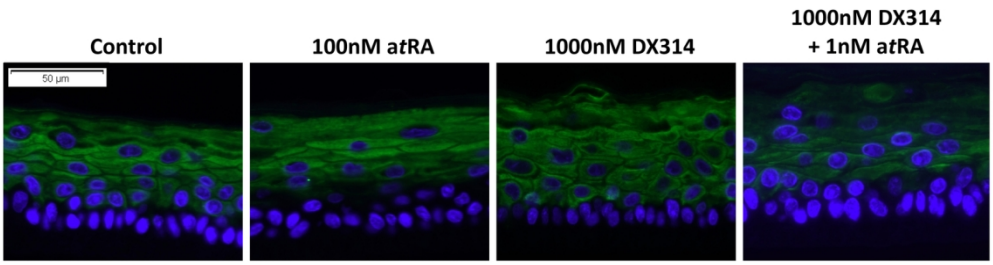

Figure S1: DX314 potentiates the effects of *at*RA on KRT10 localization in healthy RHE.
Immunofluorescent staining of KRT10 (green) localization with nuclear stain (blue) in healthy RHE treated for 4 days. Scale bar =50µm.

148x39mm (300 x 300 DPI)

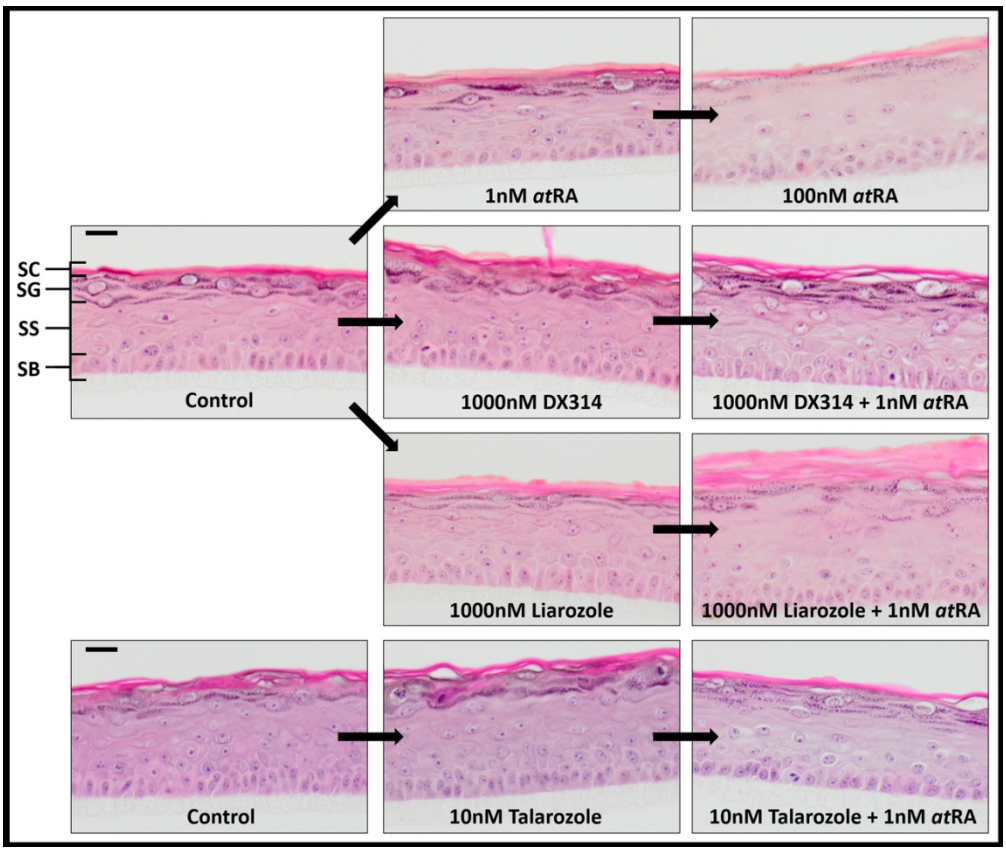

Figure S2: A*t*RA causes abnormal morphological effects in healthy RHE, which are potentiated by liarozole and talarozole, but not DX314. HE staining of healthy RHE treated for 4 days by a*t*RA or RAMBAs with, and without, a*t*RA. Scale bar =20µm. (SC, stratum corneum; SG, stratum granulosum; SS, stratum spinosum; SB, stratum basale).

110x92mm (300 x 300 DPI)

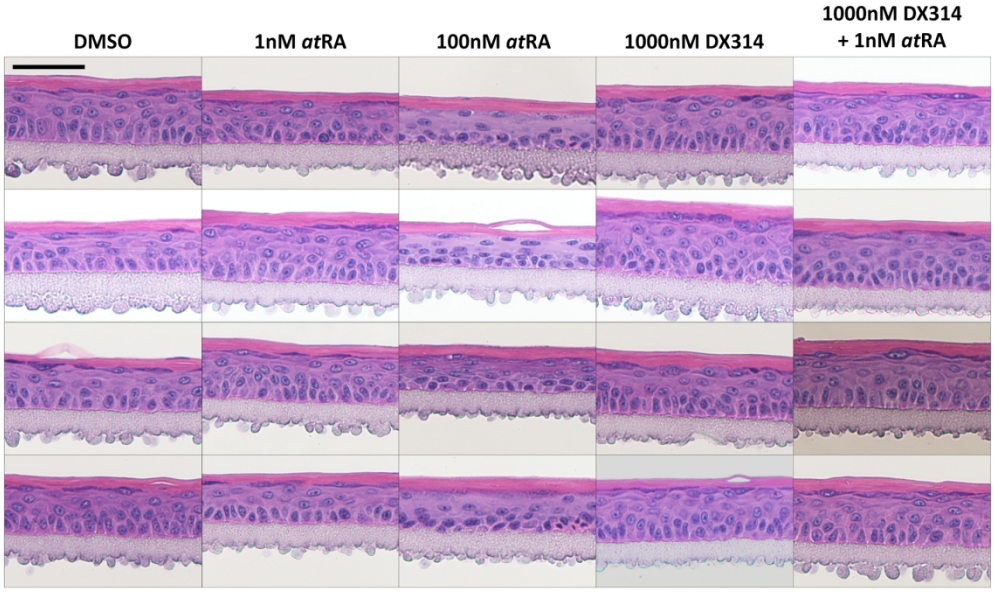

Figure S3: Tissues used in semi-quantitative analysis of relative stratum granulosum (SG) surface area. Healthy RHE were treated for 4 days before processing, HE staining, and imaging. Shown are cropped images of the samples used to determine SG surface area as a percent of total tissue surface area (**Figure 4d**). Scale bar =50µm.

169x100mm (300 x 300 DPI)

a

	DX314		Reference Ligand	
	Activation %	EC50 (nM)		
PPARα	IA	IA	50	GW 7647
PPARδ	IA	IA	1.6	GW501516
PPARγ	IA	IA	126	BRL49653
LXRβ	IA	IA	200	GW3965
RARα	IA	IA	32	Tazarotene
RARβ	IA	IA	3.2	
RARγ	IA	IA	25	
RXRβ	IA	IA	501	
AR	IA	IA	0.50	BMS 564929
GR	IA	IA	40	Dexamethasone
MR	IA	IA	0.40	Corticosterone
PR	IA	IA	251	Progesterone
ERα	IA	IA	0.016	17β-estradiol
ERβ	IA	IA	0.050	
RORα	102	538	2512	SR1078
RORγ	118	159	3981	LYC-55716

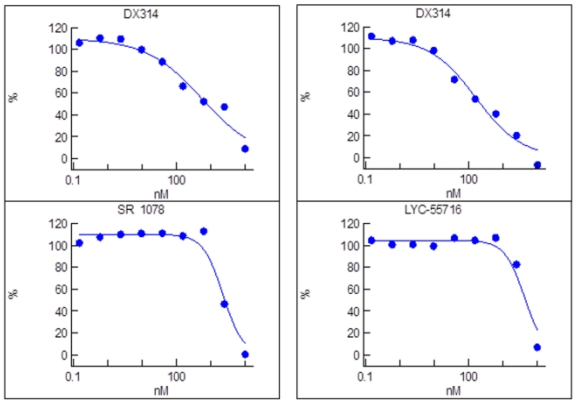

Figure S4: DX314 acts as an inverse agonist on RORα and RORγ, displays no activity on other nuclear receptors. (a) Table of EC_{50} values for DX314 and respective reference ligand. Non-linear regression of normalized **(b)** RORα and **(c)** RORγ luciferase reporter assay activity. IA = Inactive.

233x103mm (300 x 300 DPI)